



Review

# Cell Design for Improving Low-Temperature Performance of Lithium-Ion Batteries for Electric Vehicles

Jincheng Zhan <sup>1,2</sup>, Yifei Deng <sup>1,2</sup>, Jiaoyi Ren <sup>3</sup>, Yaohui Gao <sup>1,2</sup>, Yuang Liu <sup>1,2</sup>, Shun Rao <sup>1,2</sup>, Weifeng Li <sup>1,2,\*</sup>

<sup>1</sup> State Key Laboratory of Automotive Simulation and Control, Jilin University, Changchun 130022, China; zhanjc1520@mails.jlu.edu.cn (J.Z.); dengyf1520@mails.jlu.edu.cn (Y.D.); gaoyh1520@mails.jlu.edu.cn (Y.G.); liuya1520@mails.jlu.edu.cn (Y.L.); 2170702070@cnu.edu.cn (S.R.)

<sup>2</sup> College of Automotive Engineering, Jilin University, Changchun 130025, China

<sup>3</sup> College of Materials Science and Engineering, Jilin University, Changchun 130022, China; renjy1620@mails.jlu.edu.cn

\* Correspondence: liweifeng@jlu.edu.cn (W.L.); gaozh@jlu.edu.cn (Z.G.)

**Abstract:** With the rapid development of new-energy vehicles worldwide, lithium-ion batteries (LIBs) are becoming increasingly popular because of their high energy density, long cycle life, and low self-discharge rate. They are widely used in different kinds of new-energy vehicles, such as hybrid electric vehicles and battery electric vehicles. However, low-temperature ( $-20\text{--}80^\circ\text{C}$ ) environments hinder the use of LIBs by severely deteriorating their normal performance. From the perspective of material design, this review summarized and analyzed common methods of improving LIBs' performance via structure optimization and material optimization, and the future development of methods in this regard is discussed. This review is expected to provide cell design ideas for enhancing the low-temperature performance of LIBs.

**Keywords:** lithium-ion batteries; low-temperature performance; performance-improving methods



**Citation:** Zhan, J.; Deng, Y.; Ren, J.; Gao, Y.; Liu, Y.; Rao, S.; Li, W.; Gao, Z. Cell Design for Improving Low-Temperature Performance of Lithium-Ion Batteries for Electric Vehicles. *Batteries* **2023**, *9*, 373. <https://doi.org/10.3390/batteries9070373>

Academic Editor: Birger Horstmann

Received: 25 May 2023

Revised: 8 June 2023

Accepted: 6 July 2023

Published: 10 July 2023



**Copyright:** © 2023 by the authors. Licensee MDPI, Basel, Switzerland. This article is an open access article distributed under the terms and conditions of the Creative Commons Attribution (CC BY) license (<https://creativecommons.org/licenses/by/4.0/>).

## 1. Introduction

The world is facing an unprecedented energy crisis and environmental pollution [1,2]. The high demand for petroleum fuels in the automotive industry and the excessive emission of pollutants are among the important reasons for the global energy crisis and environmental pollution. Therefore, countries around the world are actively taking measures to develop new-energy vehicles to alleviate energy shortages and environmental pollution [3].

As a kind of new-energy vehicles, electric vehicles have an energy conversion rate of 75% or higher, which is considerably larger than that of conventional vehicles, and are characterized by energy savings and low pollution [4–7]; therefore, they are widely considered a promising approach to achieving a clean, efficient transportation system [8]. Electric vehicles have developed rapidly in recent years and have gradually become a global hot spot. Because lithium-ion batteries (LIBs) have a high specific energy, long life, excellent safety, fast-charging capability, low self-discharge, and eco-friendliness, a vehicle equipped with LIBs has a relatively long electric endurance mileage and can meet the power requirements of electric vehicles [9–11]. Furthermore, because LIBs can be combined with grids to store electricity from sustainable energy sources, such as photovoltaics and wind energy, LIBs have become a key part of the development of electric vehicles [10]. LIBs are also widely used to power electric vehicles because of their performance, safety, and cost advantages [12,13].

However, LIBs' performance is greatly affected by the environmental conditions, especially at low temperatures, ranging from  $-20^\circ\text{C}$  to  $-80^\circ\text{C}$ . The deterioration of LIBs' performance at low temperatures mainly manifests in the following aspects. (1) **The discharge capacity reduces.** Li et al. [14] found that, at  $-40^\circ\text{C}$ , a 1 Ah  $\text{LiNi}_{1/3}\text{Co}_{1/3}\text{Mn}_{1/3}\text{O}_2$

(NCM111) pouch cell with a conventional electrolyte retained only approximately 20% of its initial discharge capacity. (2) **The rate performance deteriorates.** Jaguemont et al. [15] reported that, when the temperature dropped to  $-25^{\circ}\text{C}$ , the discharge rate of an LIB had to be set to  $0.2\text{ C}$  or even less to maintain its room-temperature discharge capacity. In addition to the reduced energy and power output, there are also thermal safety issues due to Li plating. The main parameters to control or improve the performance of LIBs at low temperatures include ionic conductivity, impedance, the ion diffusion rate, and so on [16–19]. Zhang et al. [20] summarized the factors that deteriorate the performance of LIBs at low temperatures, which mainly include: (1) the decreased ionic conductivity and wettability of liquid electrolytes; (2) the increased intrinsic grain-boundary resistance and slow  $\text{Li}^{+}$  diffusion rate in electrodes; (3) the difficult  $\text{Li}^{+}$  dissolution and sluggish  $\text{Li}^{+}$  transport through the solid-electrolyte interphase (SEI) along with high charge-transfer resistance; (4) the occurrence of Li plating. These factors are shown in Figure 1 from Zhang et al. [20]. The first factor leads to high viscosity or solidification of the electrolyte, which hinders the ionic transport; the second factor inhibits the (de)lithiation reactions; the third one slows down the battery kinetics; the fourth one not only consumes lithium-ions, resulting in a reduction of reversible lithium-ions, but also easily causes safety problems [21,22]. The key consideration in alleviating the capacity deterioration of LIB is the sluggish kinetics of  $\text{Li}^{+}$  [23].

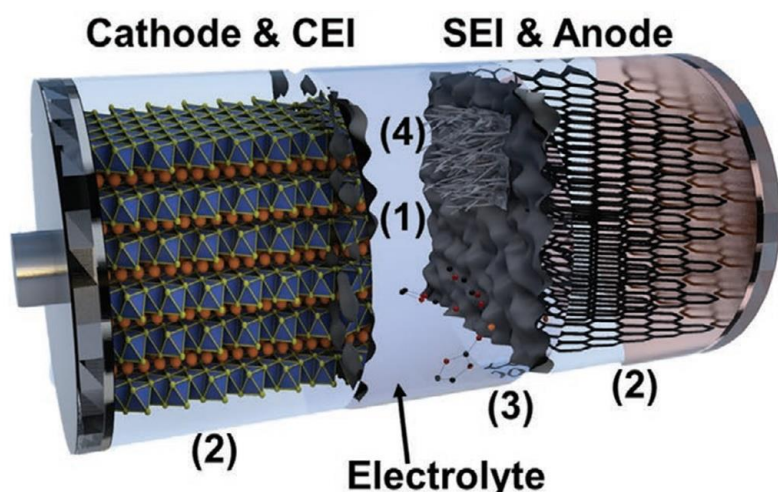


**Figure 1.** Factors deteriorating LIB performance at low temperatures [20].

In order to improve the low-temperature performance of batteries, from the perspective of the system, researchers often focus on optimizing the battery's thermal management system to improve the temperature of the battery's operating environment [8]. From the perspective of materials and cells, researchers often focus on improving the anode, cathode, and electrolyte materials, optimizing the porosity, compaction density, and thickness of the electrode, so as to essentially improve the ionic conductivity, ionic conduction rate, and diffusion rate of the battery and shorten the ionic conduction distance [20,23]. However, there are few articles summarizing the current research status of enhancing the low-temperature performance of LIBs from the perspective of cell design, including material optimization (anode, cathode, and electrolyte) and structure optimization (tortuosity and porosity). They are shown in Figure 2. They can both increase the battery discharge capacity and improve the rate performance. The optimization of anode and cathode materials can effectively reduce the charge-transfer resistance at low temperatures, shorten the diffusion distance of lithium-ions, accelerate the diffusion rate of lithium-ions and, then, enhance the diffusion kinetics of  $\text{Li}^{+}$ , improve the discharge capacity of the battery, and improve the rate performance [10,17]. The design and development of the electrolyte can reduce the freezing point of the solvent, improve the ionic conductivity, and then, increase the capacity of the battery at low temperatures, which result in a considerable improvement in the

discharge capacity of the LIBs at low temperatures [14,16]. Low electrode tortuosity and high electrode porosity improve the lithium-ion transport in an electrode; it can speed up the ion transport rate and shorten the lithium-ion transport path, effectively improving the lithium-ion transport efficiency [23].

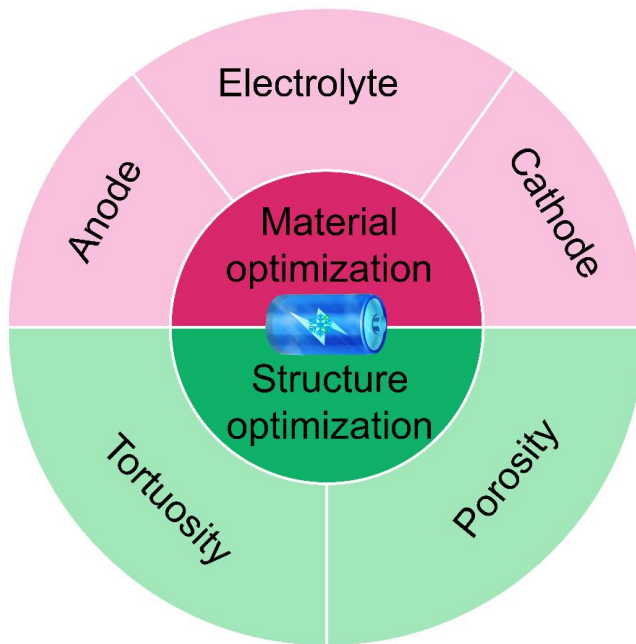


**Figure 2.** Cell design methods of enhancing LIBs' performance at low temperatures.

Focusing on LIBs for electric vehicles, this paper summarizes and analyzed published methods of improving the low-temperature performance of LIBs from the viewpoint of cell design. The possible effect of changing the battery structure on the low-temperature performance of LIBs is discussed. Next, carbon materials, lithium titanate, layered oxides, spinel-structured oxides, and other anode and cathode materials are explained. The remarkable effects of various electrolytes (including four common materials such as aqueous electrolyte and organic electrolyte) on enhancing the low-temperature performance of LIBs are then analyzed. The organic electrolyte is discussed from three aspects: solvents, lithium salts, and additives. Finally, the development opportunities for the performance-improving methods of LIBs under low-temperature conditions are given, followed by some opinions and suggestions. This review is expected to inspire further studies on enhancing the low-temperature performance of LIBs from the perspective of cell design.

## 2. Cell Fabrication/Structure Optimization

Battery components and fabrication methods affect the low-temperature capability of batteries. For example, a small electrode thickness, low electrode compaction density, and high electrode porosity can improve the transport of lithium-ions [23]. Low temperature significantly limits the ion conductivity and mobility of lithium-ion batteries [23]. However, there are relatively few studies on improving the low-temperature performance of lithium-ion batteries in battery manufacturing. Therefore, this section attempts to summarize the existing methods that can improve the ion conductivity and mobility of lithium-ion batteries, in order to provide inspiration for improving the low-temperature performance of batteries in battery manufacturing in the future.

In this section, cell structure optimization based on tortuosity and porosity is reviewed and as shown in Figure 3, this figure shows the schematic diagram and result analysis of the improvement of lithium-ion battery performance by cell structural optimization. In a low-temperature environment, compared with a thick electrode, a thin electrode can greatly improve the conduction efficiency of lithium-ions, but has inferior

energy storage potential. The electrode thickness ranges from a few tens to several hundred micrometers [24]. Zhou et al. [25] proposed the concept of the “sub-thick electrode”. The sub-thick electrode refers to the electrode with a certain minimum thickness (300–2000  $\mu\text{m}$ ) directly manufactured by chemical reaction compared with the traditional thick electrode. Wang et al. [26] have also studied the ultra-thick double-layer LiFePO<sub>4</sub> (LFP) electrode with a thickness of up to 1200  $\mu\text{m}$ . In the future high-power energy storage systems of electric vehicles, thicker electrodes will mean higher energy storage potential [27]. Data shows that, if the electrode thickness is increased from 25  $\mu\text{m}$  to 200  $\mu\text{m}$ , the proportion of inactive ingredients in the battery will be reduced from 44 wt% to 12 wt%, which means an increase in battery energy density [28]. Therefore, the development of thick electrodes with high lithium-ion conduction efficiency is promising for the applications of LIBs at low temperatures. Low electrode tortuosity and high electrode porosity improve the lithium-ion transport in an electrode [28]. According to the equation  $D_{\text{eff}} = \frac{\varepsilon}{\tau} D$  (where  $\varepsilon$  is the porosity,  $D$  is the intrinsic ionic conductivity, and  $\tau$  is the tortuosity), the effective ionic conductivity,  $D_{\text{eff}}$ , is inversely proportional to the electrode tortuosity,  $\tau$ , and proportional to the electrode porosity,  $\varepsilon$ . Ju et al. [29] quantitatively established the relationship between the tortuosity of the ferric oxide electrode and the rate capacity of the battery through experiment and theory, as shown in Figure 3A. It can be found that, with the bending from 10 to 1, the rate capacity of the battery continues to improve. Thus, the electrodes with low-tortuosity structures exhibit fast ionic transport.

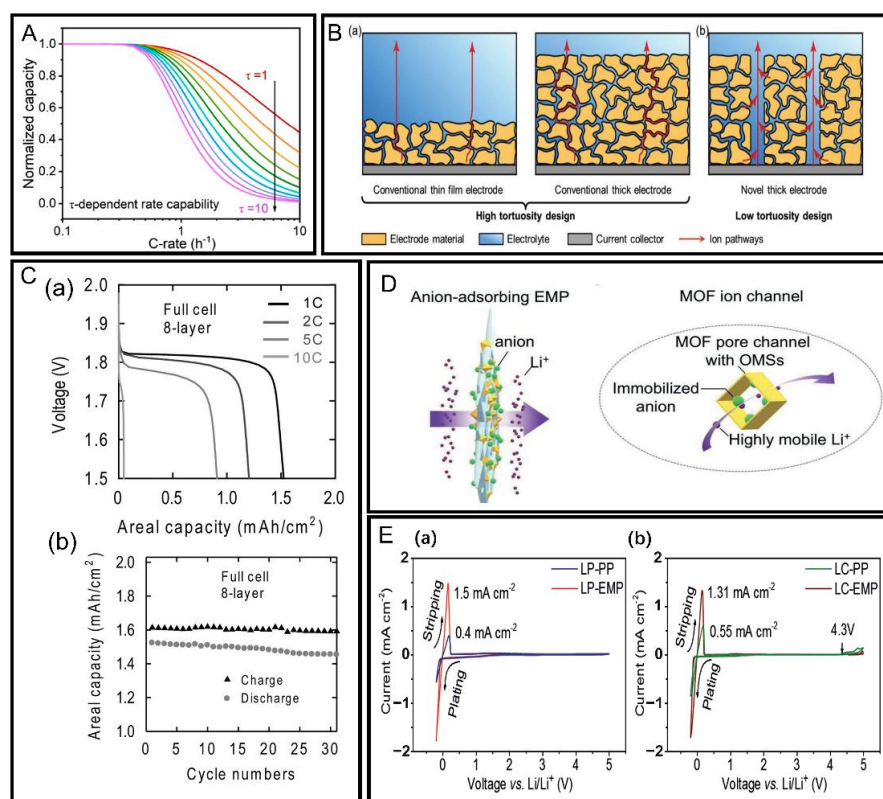


**Figure 3.** Cell fabrication/structure optimization. (A) Normalized rate ability of electrodes with different tortuosities [29]. (B) Schematic diagrams of ionic transport paths in different electrodes. (a) Traditional electrodes with inherent zigzag pore structure. (b) Thick electrodes with low-tortuosity pore structure. The red arrows indicate the shortest ionic transport pathways [28]. (C) Full voltage-areal capacity diagram and cycle performance of 3D-printed eight-layer LFP/LTO battery at different discharge rates [30]. (D) Schematics of functional EMP for adsorbing anions and facilitating lithium-ion transport [31]. (E) Electrochemical characterization of PP and EMP. (a) Ionic conductivity at various temperatures and activation energy obtained from linear fitting of the Arrhenius equation. (b) Comparison of  $t_{\text{Li}^+}$  and ionic conductivity [31].

The close, random packing of electrode elements in traditional thick electrode structures (Figure 3B(a) [28]) usually results in electrodes with tortuous pore structures, which significantly hinders their penetration by electrolytes, considerably increases the ionic transport distance, and reduces ionic transport efficiency. As shown in Figure 3B(b) [28], Kuang et al. [28] developed a low-tortuosity pore structure to enhance the ionic transport in an electrode at low temperatures. The lithium-ion transport path in the innovative low-tortuosity electrode structure shortened, which effectively improved the lithium-ion transport efficiency.

Sun et al. [30] created a low-tortuosity electrode structure through 3D printing, which effectively improved the transport efficiency of lithium-ions. They uniformly dispersed  $\text{Li}_4\text{Ti}_5\text{O}_{12}$  (LTO) and LFP nanoparticles in a mixture of water, glycerin, ethylene glycol (EtG), and viscosifiers to produce a printable ink with a 60 wt% solid load. They used this ink for the 3D printing, followed by drying and annealing, of an eight-layer LTO/LFP lithium-ion microbattery electrode structure with a low bending degree and a high aspect ratio. To study the electrochemical performance of the microbattery, Sun et al. [30] printed 8 and 16 layers of 3D-IMA (960 × 800  $\mu\text{m}$ , 60  $\mu\text{m}$  electrode width, 50  $\mu\text{m}$  spacing) on a glass substrate and then measured the voltage–areal capacity curve of the microbattery at different discharge rates, as shown in Figure 3C(a) [30]. The areal capacity at 1 C was 1.5  $\text{mAh cm}^{-2}$ , which agreed well with the theoretical results for LFP and LTO half-cells. Moreover, the cycle life of 3D-IMA was determined, and the results are shown in Figure 3C(b) [30]. The minimum attenuation of the capacity reached 30 cycles, showing a good cycle life.

High porosity can improve the lithium-ion transport in an electrode. High-porosity structures have been fabricated using different approaches, such as the subtractive design method, wherein a porous structure is introduced into the electrode by reducing some of the components of the electrode precursor [28]. During the drying process in traditional electrode manufacturing, by removing the solvent components in the electrode, an interconnected pore network is formed to improve the ion transport efficiency. However, this random electrode structure manufacturing approach increases tortuosity. Researchers have explored the orderly directional introduction of pore structures into electrodes to reduce tortuosity. For example, the transport efficiency of lithium-ions can also be improved using magnetic materials and external magnetic fields [28,32]. In such approaches, active electrode materials with anisotropic structures, such as graphite anodes, are modified and oriented [28,32] and then decorated with superparamagnetic ferric oxide ( $\text{Fe}_3\text{O}_4$ ) nanoparticles. To induce a sensitive magnetic response in such materials, Billaud et al. [33] applied an external magnetic field to the electrode slurry to control the orientation of graphite electrode sheets along the magnetic field and form an out-of-plane-aligned architecture. This unique structure decreased the lithium-ion transport distance and resulted in an ultrathick 10  $\text{mg cm}^{-2}$  graphite electrode (200  $\mu\text{m}$  thickness), which increased the specific charge capacity threefold.

Zhang et al. [31] used electrospinning to prepare a new composite separator called electrospun metal–organic framework (MOF)–poly (vinyl alcohol) composite membranes (EMP), which contains MOF particles and polyvinyl alcohol. The common polypropylene (PP) LIB separator was selected as the control group for experimental verification. They measured the  $\text{Li}^+$  conductivity of the composite separator via electrochemical impedance spectroscopy. As seen in Figure 3D [31], at an ambient temperature of 30 °C, the ionic conductivities of 1 M  $\text{LiPF}_6$  in the ethylene carbonate/diethyl carbonate LP’s EMP (LP-EMP) and 1 M  $\text{LiClO}_4$  in the propylene carbonate (LC)’s EMP (LC-EMP) were 2.9 and 1.9  $\text{mS cm}^{-1}$ , respectively. In contrast, the ionic conductivities of LP-PP and LC-PP were only 0.7  $\text{mS cm}^{-1}$  and 0.5  $\text{mS cm}^{-1}$ , respectively. Besides, the activation energy of LP-EMP and LC-EMP were lower than the latter with PP. As shown in Figure 3E [31], the lithium-ion transference numbers  $t_{\text{Li}^+}$  of LP-PP and LC-PP were 0.37 and 0.49, respectively, whereas those of LP-EMP and LC-EMP were significantly higher (0.59 and 0.79, respectively). In LP and LC, when PP was replaced with EMP, the conductivity of lithium-ions increased 467% and 433%, respectively, which significantly improved the battery conductivity. These findings indicated

that MOF particles containing open metal sites could spontaneously adsorb anions and effectively transport lithium-ions in the electrolyte, thereby significantly increasing  $t_{Li^+}$  (up to 0.79) and lithium-ion conductivity [31]. Therefore, the use of such MOF particles can provide new ideas for improving the performance of LIBs at low temperatures.

In general, cell fabrication significantly influences the low-temperature performance of batteries, but further study is needed to explore solutions and measures to improve conductivity. Through Table 1, it can be seen that, with the low tortuosity of the electrode, the development of a new EMP composite separator significantly improves the conduction efficiency and ion mobility of lithium-ions, increasing by 300% and 460%, respectively [31,33]. Besides, the directional introduction of pores also increases the capacitance by three-times. They proved that, in the future, we can take an important step in improving the rate performance and capacity performance of LIBs at low temperatures from the perspective of low-tortuosity electrodes and directional porous electrodes.

**Table 1.** A summary of tests and results related to cell fabrication/structure optimization.

| Methods                                     | Chemistry   | Test  | Results   | Ref. |
|---|---|---|---|------|
| Cell fabrication/<br>structure optimization | 1 M LiPF <sub>6</sub> + DEC/EC (1:1<br>vol), 1 M (homemade)<br>LiClO <sub>4</sub> in PC | 30 °C, EIS  | The ionic conductivity is<br>300% higher than before  | [31] |
|   | Li   electrolyte   Li cells<br>half-cells   | Potentiostatic polarization<br>at voltage bias of 20 mV<br>Test: AC impedance and DC<br>potentiostatic polarization<br>measurements<br>C/10 and 1 C, rate<br>capability tests | The $t_{Li^+}$ is 460% higher than<br>before          | [31] |
|   |   |   | Increase the specific charge<br>capacity by threefold | [33] |

### 3. Material Optimization

Studying and improving cell materials, such as anode, cathode, and electrolyte materials, can effectively improve the low-temperature performance of LIBs (Figure 4) [20,23]. This section mainly introduces studies on enhancing such LIB performance by enhancing the cell materials.

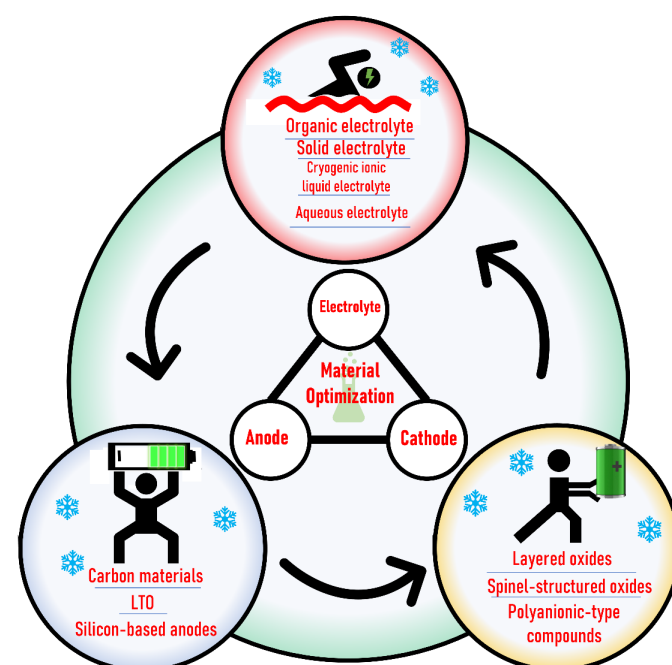


**Figure 4.** Classification of material optimization.

### 3.1. Anode Materials

**Carbon materials.** Graphite is the most-commonly used LIB anode material, but its performance is significantly affected by low temperatures. At sub-zero temperatures, the intercalation/de-intercalation kinetics of the graphite anode are very slow, resulting in a significant loss of battery capacity. Low temperatures inevitably lead to a rapid increase in charge-transfer resistance [34–36]. According to U.S. ARL, when the temperature drops from  $-30^{\circ}\text{C}$  to  $-40^{\circ}\text{C}$ , the charge-transfer resistance of the graphite electrode battery increases by 2000-times [37]. In addition, graphite anodes are prone to lithium dendrites when charged at low temperatures, which may short-circuit the battery and pose a great challenge to battery safety [36]. Figure 5 illustrates the improvement effect on the low-temperature performance of LIBs for the cases mentioned in this section. Prelithiation treatment can enhance the low-temperature properties of graphite. The prelithiation treatment can prevent the negative-electrode-form SEI film from consuming the lithium-ions removed from the positive electrode, but obtain lithium-ions from other places, so as to ensure that the lithium-ions removed from the positive electrode will not be wasted in the formation of the negative SEI film [37]. Liu et al. [38] designed a  $\text{Li}_3\text{V}_2(\text{PO}_4)_3$  (LVP)/hard carbon battery, and its initial charge was used for prelithiation. The battery showed a capacity retention rate of over 67% at  $-40^{\circ}\text{C}$  relative to that measured at room-temperature; this figure is far superior to that of traditional LIBs (Figure 5A [38]). Kim et al. [39] prepared a composite composition of edge-plane-activated graphite and an a-Si nanolayer (SEAG) as a hybrid anode with good low-temperature properties, and its initial coulombic efficiency reached 93.8%. They measured the battery's capacity retention using a battery circulator (TOSCAT-3100, Toyo system). At a current density of  $1.75 \text{ mA cm}^{-2}$ , the capacity retention rate of this anode material in 50 cycles was 99.3% (Figure 5B [39]). Nano-tin-doped particles can also improve the working ability of graphite at low temperatures [40]. Yan et al. [40] doped graphite with nano-tin as the anode ( $\text{Sn/EtG}$ ) of an LIB. In their experiment, they found that the anode material decreased the charge-transfer resistance of the cell after 10 cycles at  $-20^{\circ}\text{C}$ . As shown in Figure 5C [40], the charge-transfer resistance of the anode material increased from  $10^2$  to  $10^4 \Omega$  as the temperature dropped from  $25^{\circ}\text{C}$  to  $-20^{\circ}\text{C}$ , whereas the charge-transfer resistance of a common graphite anode was too large to be measured at  $-20^{\circ}\text{C}$ . Zhang et al. [41] developed a 3D nitrogen-doped porous carbon frame with a nitrogen content of 19% by sintering nitrogen-doped carbon dots at  $800^{\circ}\text{C}$ . The specific capacity of the cell reached  $840 \text{ mAh g}^{-1}$  after 1000 cycles. The experiment was carried out with Land CT2001A at a current density of  $2 \text{ Ag}^{-1}$  from 0.01 to 3 V. Similar to silicon, nitrogen, and tin, Cu has been used to coat a graphite oxide anode [42]. The experiment in this previous study proved that this method could improve the battery capacity at low temperatures; however, the Cu coating may have compromised the cell capacity at  $0^{\circ}\text{C}$  to  $20^{\circ}\text{C}$  [42]. In short, researchers have made much exploration on how to improve the low-temperature performance of carbon material anode batteries, among which prelithiation treatment and anode surface modification are currently more-commonly used and -effective methods.

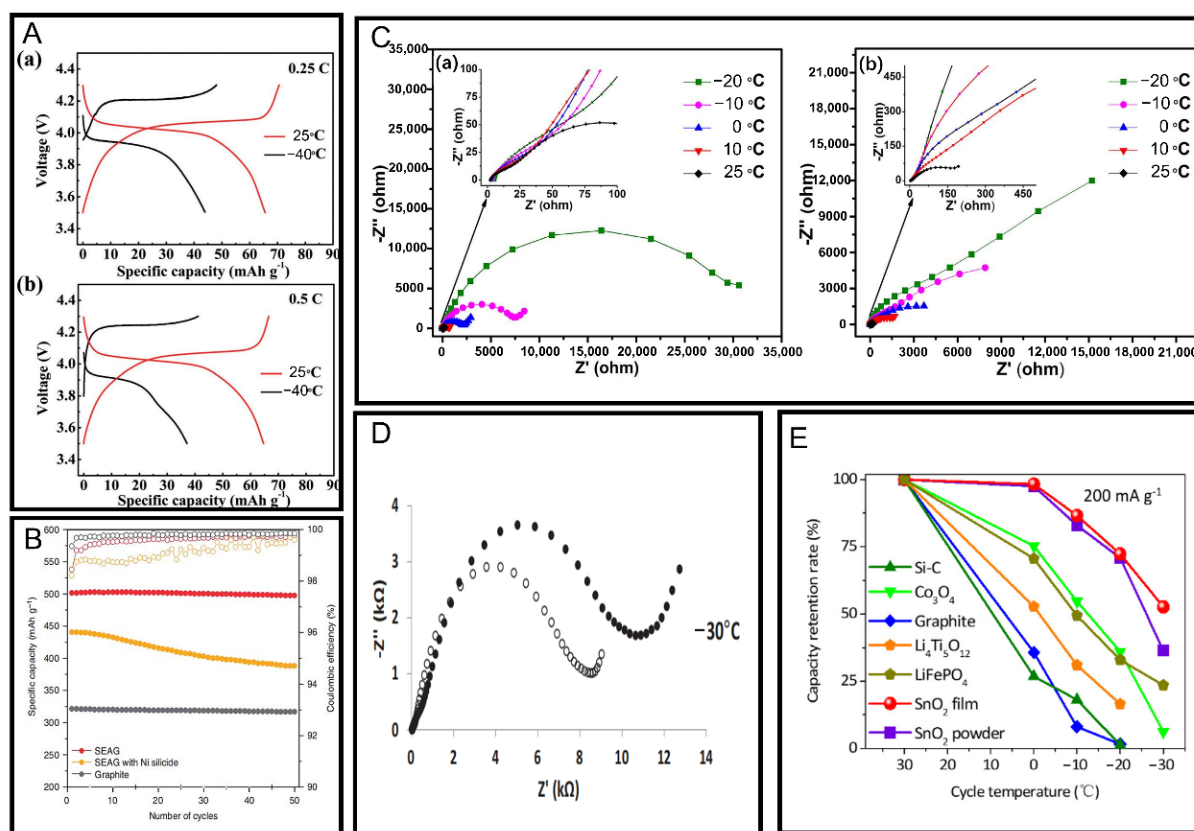


**Figure 5.** Anode design and improvement. (A) Galvanostatic charge/discharge curves at rates of (a) 0.25 C and (b) 0.5 C at voltages of 3.5 to 4.3 V at  $-40\text{ }^{\circ}\text{C}$  [38]. (B) Reversible capacity and cycling coulombic efficiency of SEAG and of graphite and SEAG with Ni silicide in over 50 cycles [39]. (C) Nyquist plots of (a) Sn/EtG electrode and (b) graphite electrode at different temperatures [40]. (D) Nyquist plots for Si/Li (hollow dots) and graphite/Li cells (full dots) at  $-30\text{ }^{\circ}\text{C}$  [43]. (E) Capacity retention rate of different materials with temperature [44].

**Lithium titanate.** The LTO structure is stable and enables lithium-ions to be deintercalated during (de-)lithiation [37]. The lattice change of LTO before and after phase transition is not obvious, which can be considered as zero strain, which is an important reason why LTO is considered to be a promising anode material [37,45–48]. However, the ion diffusion coefficient of LTO is not high ( $10^{-9}$  to  $10^{-13}\text{ cm}^2\text{s}^{-1}$ ) and the conductivity is low ( $10^{-9}\text{ S cm}^{-1}$ ), which means that the low-temperature performance of LTO will be greatly limited [46]. The LTO particle size can be changed to reduce the interface resistance and enhance the properties of the cell [49]. Kallio et al. [49] explored the low-temperature performance of LTO particles with different sizes, including particles with a small primary particle size (LTO-SP, 150 nm,  $22\text{ m}^2\text{ g}^{-1}$  surface area) and particles with a large primary particle size (LTO-LP, 225 nm,  $7\text{ m}^2\text{ g}^{-1}$  surface area). They tested the charge/discharge capacity of LTO half cells at  $-20\text{ }^{\circ}\text{C}$  and 0.1 C with the Neware battery cycler. The half cells were charged and discharged at constant current at a voltage range of 1.1 and 2.5 V, and they kept the temperature stable for an hour before the test began. The experiment verified that the capacity of the small particles (large surface area) was approximately 31% higher than that of the large particles. The reason may be that, at low temperatures, the smaller particle size will significantly increase the number of surface sites for lithium insertion and shorten the diffusion path of lithium-ions and may form a denser composite structure, which is very favorable for improving the capacity of the battery [49].

**Silicon-based anodes.** The theoretical capacity of silicon anodes is very high, especially at subzero temperatures; its capacity is much higher than that of graphite [37]. Therefore, silicon anodes are considered to be a method to improve the low-temperature

performance of graphite anode batteries. Markevich et al. [43] used an Arbin model BT2000 battery tester and Autolab System to analyze the performance of a silicon anode in a 1 M LiPF<sub>6</sub> fluoroethylene carbonate (FEC)/dimethyl carbonate (DMC) (1:4 vol) solution at  $-30^{\circ}\text{C}$ . They found that the charging capacity of the silicon anode was 28.8-times that of the graphite anode. In addition, the team also measured the electrochemical impedance spectra (EIS) of two different anode cells at  $-30^{\circ}\text{C}$  with a potentiostat-galvanostat Model 128 N Autolab in the frequency range of 100 kHz–1.7 mHz [43]. As can be seen from Figure 5D [43], the resistance of the silicon anode was significantly lower than that of the graphite anode, which is one of the reasons for the superior capacity performance of silicon over graphite. Subburaj et al. [50] assembled a Si/LiNi<sub>0.8</sub>Co<sub>0.15</sub>Al<sub>0.05</sub>O<sub>2</sub> pouch cell and tested its electrochemical characteristics. At  $-40^{\circ}\text{C}$ , the discharge capacity of the cell exceeded 700 mAh g<sup>-1</sup>, which was 65% of that at  $20^{\circ}\text{C}$ . However, silicon-based anodes may have certain problems. For example, the volume expansion of silicon electrodes is severe, even reaching 300% [50]. Therefore, methods such as the use of nanostructures and porous structures have been implemented to enhance the practicality of silicon anodes at low temperatures [51,52].

In addition to the three common anode materials mentioned above, Sn, Ge, and other elements are often used as battery anodes [53–55]. SnO<sub>2</sub> has a natural advantage for low-temperature applications. Low temperatures inhibit Sn coarsening and maintain the high reversibility of the SnO<sub>2</sub> alloying and conversion reactions, thus ensuring stable capacity [44]. Tan et al. [44] experimentally compared the performance of a tin oxide anode and other anodes, such as graphite, at  $-10^{\circ}\text{C}$ . The electrolytes they used were 1 M LiFP<sub>6</sub> in a mixture of EC, PC, and EMC with a volume ratio of 1:1:2 and 5 wt% FEC additives. After 10 cycles, the capacity retention rate of the tin oxide electrode at  $-10^{\circ}\text{C}$  was 82.9% of that at  $30^{\circ}\text{C}$  (Figure 5E [44]). By contrast, the capacity retention rate of the graphite anode under the same conditions was only 10.1%, which was considerably lower than that of the tin oxide anode [44].

Table 2 summarizes the methods for improving the anode, including prelithiation treatment, particle size reduction, exploration of new anode materials, etc. Prelithiation treatment or exploration of new materials can significantly improve the performance rate and capacity of the battery. For example, at  $-40^{\circ}\text{C}$ , prelithiation treatment can maintain 67% capacity of the batteries that could not work [38], and the capacity of some new anode materials has been studied to be tens of times higher than that of graphite, such as Si [43] or SnO<sub>2</sub> [44]. However, the improvement of the low-temperature performance of the battery by reducing the particle size was not great, such as reducing the particle size of the LTO anode, which can only increase the capacity by up to 31% [49]. In fact, no matter what method, there are some limitations, which still need to be further explored.

**Table 2.** A summary of tests and results related to anode materials.

| Anode  | Chemistry   | Methods                 | Action Mechanism  | Test  | Results  | Ref. |
|--------|---|-------------------------|---|---|--|------|
| Carbon | 1 M LiPF <sub>6</sub> + EMC/DMC/EC (1:1:1 vol), hard carbon/LVP cells | Prelithiation treatment | The lithium-ions needed to make the negative electrode form an SEI film are obtained from somewhere other than the positive electrode | $-40^{\circ}\text{C}$ , 0.25 C, 3.5 to 4.3 V, charge-discharge test | Without improvement: cannot work<br>After improvement: capacity retention rate exceeds 67% | [38] |

**Table 2.** Cont.

| Anode            | Chemistry   | Methods                                  | Action Mechanism   | Test  | Results   | Ref. |
|------------------|---|--|--|---|---|------|
|                  | 1 M LiPF <sub>6</sub> + DMC/EC (1:1 vol), graphite CR2032-type coin cells                               | Embedding nano-Sn                        | The nano-Sn particles/graphene/2D graphene alternating stack structure will shorten the diffusion distance of lithium-ions   | –20 °C, EIS   | After improvement: the charge-transfer resistance is 10 <sup>4</sup> Ω<br>Without improvement: too large to measure | [40] |
| LTO              | 1 M LiPF <sub>6</sub> + DMC/EC (1:1 wt), LFP/LTO full cells   | Reducing the particle size               | Smaller particle sizes will increase the number of surface sites for lithium insertion, shorten the diffusion path of lithium-ions, and may form denser composite structures | –20 °C, 0.1 C, 1 to 2.6 V, charge-discharge test                | The capacity of small particles is about 31% higher than that of large particles                                    | [49] |
| Si               | 1 M LiPF <sub>6</sub> + FEC/DMC (1:4 vol), Si/Li cells  | Use silicon instead of graphite          | The charge-transfer resistance of silicon material is smaller than that of graphite at zero temperature, and the diffusion rate of lithium-ion is faster                     | –30 °C, 0.25 C, 0.24 mA cm <sup>−2</sup> , charge capacity test | The capacity of Si anode is 28.8-times that of graphite anode   | [43] |
| SnO <sub>2</sub> | 1 M LiPF <sub>6</sub> + EC/PC/EMC (1:1:2 vol) + FEC (5 wt%), SnO <sub>2</sub> 2016 coin-type half-cells | Use SnO <sub>2</sub> instead of graphite | The low temperature inhibits Sn coarsening to maintain the high reversibility of the SnO <sub>2</sub> alloying and conversion reactions, ensuring a stable capacity          | –10 °C, capacity retention rate test                            | The capacity retention is 680% higher than that of graphite anode   | [44] |

Existing research indicates that carbon materials are the most-common anode materials. However, graphite and other such materials are significantly affected by low temperatures; in particular, the charge-transfer resistance rapidly increases with a decrease in temperature [34–36]. In addition, lithium plating is a major problem in carbon materials. Although mitigated via prelithiation, coating, and other methods, these problems still need further improvement [36]. Compared with carbon materials, lithium titanate is more stable and can, thus, enhance the low-temperature properties of LIBs [37]. However, the high working voltage and low energy density of this material limit its application to LIBs [51]. Silicon-based anodes exhibit good application potential at low temperatures [37]. Nevertheless, their severe volume expansion should be resolved, and studies on this subject are limited [49]. Hence, enhancing the low-temperature properties of LIBs by optimizing their anode materials has broad research prospects.

### 3.2. Cathode Materials

Cathodes may not be the most-critical factor resulting in the poor low-temperature properties of LIBs [20]; instead, they are essential parts of LIBs and are the core of Li<sup>+</sup> exchange. They also affect the working ability of cells at low temperatures, so cathode materials should be studied to improve the cryogenic properties of cells [20]. At present, reducing the particle sizes of materials [20,56], adding coatings [57,58], and doping elements [59] are important ways to enhance the low-temperature performance of batteries

from the cathode perspective. Figure 6 shows the improvement in LIBs' performance at low temperatures after applying these methods.

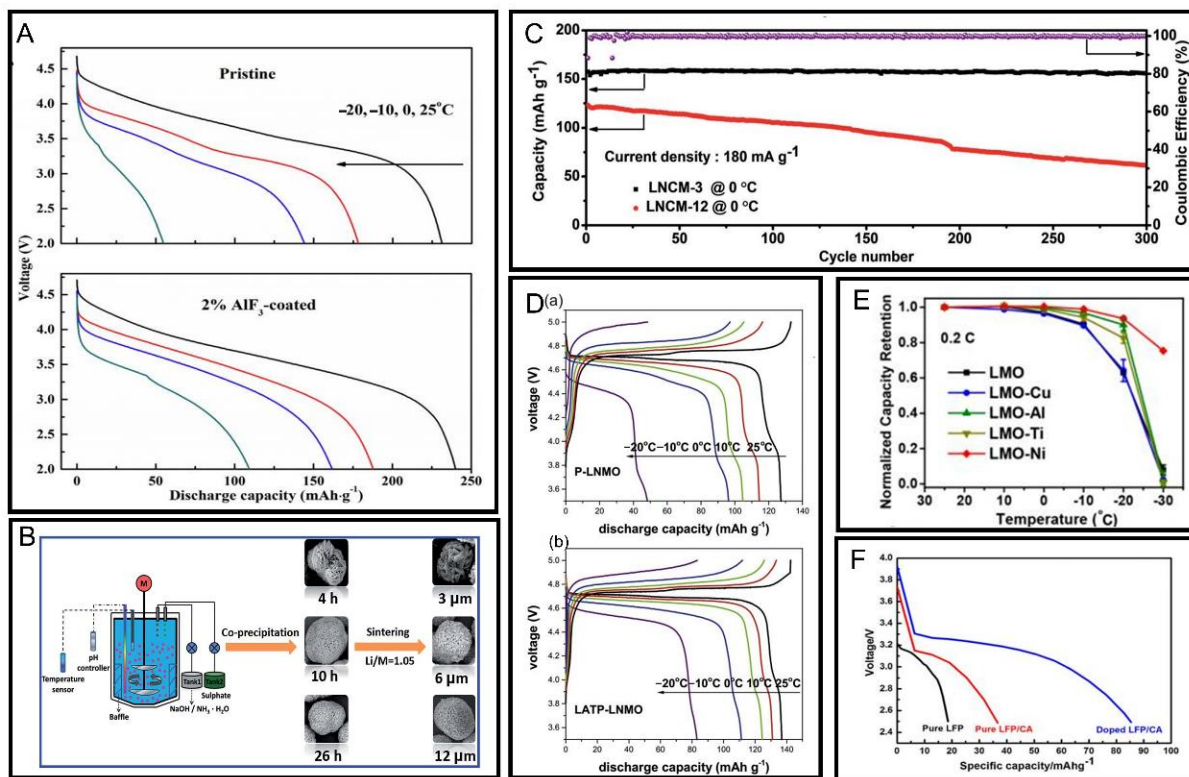


**Figure 6.** Cathode design and improvement. (A) Discharge curves (0.1 C) of primeval and 2%  $\text{AlF}_3$ -coated  $\text{Li}_{1.2}\text{Ni}_{0.13}\text{Co}_{0.13}\text{Mn}_{0.54}\text{O}_2$  at different temperatures [60]. (B) Schematic diagrams of the synthesis of different types of NCM622 [61]. (C) Cycling performance of LNCM-3 (3  $\mu\text{m}$  particle size) and LNCM-12 (12  $\mu\text{m}$  particle size) at 0 °C between 3 and 4.4 V [61]. (D) Curves of initial charge–discharge capacity of (a) P-LNMO and (b) LATP-LNMO [62]. (E) Normalized capacity retention of bare and modified LMO with temperature [63]. (F) Discharge curves of modified LFP/CA (carbon aerogel), pure LFP/CA, and pure LFP at 10 °C and -20 °C [64].

**Layered oxides.** Lithium cobalt oxide is a typical layered oxide, but its kinetic characteristics are poor. At -40 °C, the energy density of lithium cobalt oxide cathodes is only 5% of that at 20 °C [65]. In addition, NCM is a layered oxide similar to the structure of lithium cobalt oxide. During the charging process of the NCM cathode battery, the electrolyte is easily decomposed due to the instability of  $\text{Ni}^{4+}$ , and the product will cover the NCM electrode, which will seriously affect the migration of  $\text{Li}^+$ . In other words, the instability of  $\text{Ni}^{4+}$  will lead to an increase in the internal resistance of the battery, which has a significant impact on the performance of the battery at low temperatures [66]. Tan et al. [67] coated NCM111 with glassy lithium borate ( $\text{Li}_3\text{BO}_3$ ) sized approximately 8 nm. They used a charge–discharge apparatus to charge and discharge the battery at a rate of 0.2 C between 2.5 and 4.5 V to measure the battery's capacity. During cycling at 0.2 C and -40 °C, the specific capacity of the electrode coated with lithium borate was 65  $\text{mAh g}^{-1}$  higher than that of an uncoated electrode. Moreover, the charging voltage of the lithium borate-coated battery was the same as that of the ordinary battery at the same capacity, but the former had a higher discharging voltage [67]. This was because the glassy lithium borate coating protected the cathode surface from the liquid electrolyte and unnecessary side reactions, thus reducing the polarization of the cell.  $\text{Li}_3\text{BO}_3$  can also be deposited on  $\text{Li}_{1.2}\text{Ni}_{0.2}\text{Mn}_{0.6}\text{O}_2$  particles to form coatings that have an appropriate thickness and can protect cathodes from HF attacks and ensure rapid  $\text{Li}^+$  transport [67]. In addition, the team's analysis of EIS showed that the B-coating can greatly reduce the contact between the active substance

and the electrolyte, thus reducing the charge-transfer resistance at low temperatures and increasing the ion diffusion coefficient, which is another reason why this method can improve the low-temperature performance of the battery [67]. Zhao et al. [60] coated  $\text{Li}_{1.2}\text{Ni}_{0.13}\text{Co}_{0.13}\text{Mn}_{0.54}\text{O}_2$  with 2% aluminum fluoride. The batteries were charged and discharged between 2 and 8 V to test their capacity. As shown in Figure 6A [60], at  $-20^\circ\text{C}$ , the capacity of the cathode coated with aluminum fluoride was approximately two-times that of an uncoated cathode. However, at  $25^\circ\text{C}$ , the coating only increased the discharge capacity by about 4.5%. Therefore, aluminum fluoride coating is an effective method to improve the performance of LIBs at low temperature. The spinel structure generated by the aluminum fluoride coating on the cathode material improved the electron migration, and the presence of  $\text{LiAlO}_2$  on the coating sample enhanced the lithium diffusion kinetics, which may be the reason for the effectiveness of this method [60]. Moreover, decreasing the material particle size can enhance the characteristic of layered oxide cathodes at low temperatures [20,61]. Sun et al. [61] studied three  $\text{LiNi}_{0.6}\text{Co}_{0.2}\text{Mn}_{0.2}\text{O}_2$  (NCM622) materials with different nanostructures, particle sizes, pore distributions, and specific surface areas. Their synthesis process diagram is shown in Figure 6B [61]. The three modified cathodes enhanced the low-temperature performance of the cells, and the NCM622 material with the smallest particle size exhibited the most-remarkable improvement. The initial coulombic efficiency of the NCM622 material with a particle size of 3  $\mu\text{m}$  reached 94.9%, and after 300 cycles at  $0^\circ\text{C}$ , its capacity retention rate was 100% (Figure 6C [61]). Element doping is also an effective way to enhance cell performance [59]. For example, Ti doping can change the lattice parameters of cathodes during charging and discharging and reduce impedance, thereby enhancing the low-temperature properties of cells [68]. Li et al. [68] charged and discharged the batteries between 2.8 and 4.25 V and tested its discharge capacity. At  $-20^\circ\text{C}$ , the discharge capacities of a Ti-doped NCM111 cathode were 51.3, 78.5, 101.8, and 122.4  $\text{mAh g}^{-1}$  at 5, 1, 0.2, and 0.1 C, respectively, and the discharge capacities of a cathode without Ti were 118.8, 96.3, 67.7, and 30.1  $\text{mAh g}^{-1}$ , respectively, under the same conditions.

**Spinel-structured oxides.** Spinel-structured oxides have excellent rate capability and physical stability. However, the charge-transfer resistance of this material increases exponentially with the decrease of temperature, and its low-temperature performance is much worse than that at room-temperature. [37,69]. Bi et al. [62] coated the structure surface of  $\text{LiNi}_{0.5}\text{Mn}_{1.5}\text{O}_4$  (LNMO) with a continuous layer of  $\text{Li}_2\text{O}-\text{Al}_2\text{O}_3-\text{TiO}_2-\text{P}_2\text{O}_5$  (LATP), which improved the performance of LNMO. They made electrochemical measurements of the batteries between voltage windows of 3.5 and 5 V using the CT2001A battery test system. The result showed that the LATP-coated electrode (LATP-LNMO) helped reduce polarization at  $-20^\circ\text{C}$ , and its energy density at this temperature far exceeded that of an uncoated electrode (P-LNMO). The initial charge-discharge curves of the LATP-coated and uncoated cells are shown in Figure 6D [62]. Regardless of temperature, the discharge capacity of the coated electrode was high, and the electrochemical performance of the cell was remarkably improved by the LATP coating when the temperature was very low. The discharge capacity of the LATP-LNMO cathode was 82.24  $\text{mAh g}^{-1}$  at  $-20^\circ\text{C}$ , which was considerably higher than that of the uncoated cathode (48.10  $\text{mAh g}^{-1}$ ). In addition, the EIS showed that the charge-transfer resistance increased rapidly with decreasing temperature, but the charge-transfer resistance of the cells with LTAP coating was only about one-tenth of that of the uncoated cells at  $-20^\circ\text{C}$  (at  $25^\circ\text{C}$ , the charge-transfer resistance of the two was of the same order of magnitude, with a difference of less than 30  $\Omega$ ), indicating that the LTAP coating was favorable for charge-transfer at low temperatures [62]. Zhang et al. [63] doped the surface of  $\text{LiMn}_2\text{O}_4$  (LMO) with nickel, which reduced the charge-transfer barrier and inhibited the capacity loss caused by a drop in temperature. As shown in Figure 6E [63], the capacity retention rate of the Ni-doped LMO was significantly high at low temperatures (approximately 90% at  $-20^\circ\text{C}$ ), whereas that of an undoped LMO was only approximately 65%.

**Polyanionic compounds.** LFP is a typical polyanionic compound with low cost and good thermal stability, but its conductivity ( $10^{-9}$  S cm $^{-1}$ ) and lithium-ion diffusion coefficient ( $10^{-14}$ – $10^{-16}$  cm $^2$  S $^{-1}$ ) are relatively low, resulting in the poor low-temperature performance and rate performance of LFP [20,70–75]. Zhang et al. [64] added Mg and La ions into LFP, and the CT2001A battery test system was used to test the charging and discharging capacity of this cathode and a pure LFP cathode –20 °C and 10 C between 3.5 and 5 V voltage windows, and the measurement curve is shown in Figure 6F [64]. The cathode discharge capacity after La and Mg doping was 85.4 mAh g $^{-1}$ , which was substantially higher than that of the pure LFP. At the same time, Zhang et al. [64] also used the CHI604B electrochemical station to perform the EIS. At –20 °C, the charge-transfer resistance of the pure LFP electrode was as high as 1431 Ω, while that of the doped LFP electrode was only 391.4 Ω. The conductivity of the pure LFP electrode was obviously improved, which can explain the reason why doping La and Mg elements can improve the performance of the LFP electrode [64]. Cui et al. [76] prepared a carbon-coated, phosphorus-doped LFP/C-P composite material as a battery cathode and tested the rate properties of a pristine commercial LFP cell, a pristine synthetic LFP cell, and the synthetic LFP/C-P composite at different temperatures. The experiment was carried out in a 2001T battery measurement system with a voltage range of 2.7–4.2 V. The experimental results showed that the rate performance of the LFP/C-P composite was excellent compared to that of the uncoated materials at any temperature. For example, at 0 °C and 1.5 C, the specific capacity of the battery containing LFP/C-P was 142.6 mAh g $^{-1}$ , whereas that of the pristine commercial LFP battery was approximately 110 mAh g $^{-1}$ . Moreover, at –25 °C, the specific capacity of the LFP/C-P cell was still approximately 40 mAh g $^{-1}$  higher than that of the pristine commercial LFP cell [76]. C coating and P doping can alleviate the corrosion of the electrolyte on the cathode and can also establish a certain number of interconnecting channels, shorten the diffusion path of lithium-ions, and then, improve the capacity retention rate and rate performance of the battery at low temperatures [76]. In addition to the above methods, reducing the material particle size can accelerate the solid diffusion of LFP. For example, an LFP/C cell with a small particle size can shorten the transport paths of the ions, thus improving the solid diffusion kinetics [23]. However, this method may lead to side reactions [23,77]. LVP is also a polyanionic compound commonly used as a cell cathode material, and its theoretical capacity is higher than that of LFP [78,79]. Compared with LFP, LVP is more conducive to the extraction/intercalation of lithium-ions [79], and coating it with carbon further improves its low-temperature performance [80]. Luo et al. [80] prepared an LVP cell coated with hierarchical carbon and verified that the coating improved the rate performance and cycle stability of the cell at –20 °C.

Vanadium oxides, Ni-based Prussian blue, and others can also be used as LIB cathode materials [81,82]. For example, V<sub>2</sub>O<sub>5</sub> has a layered structure and high lithium insertion potential [82]. Sides et al. [83] prepared a nanoscale (70 nm) V<sub>2</sub>O<sub>50</sub>. At –20 °C, the cathode material shortened the transport distance of Li $^{+}$ , thus enhancing the low-temperature performance.

Most studies on low-temperature cathodes focus on improving their lithium-ion transport performance, conductivity, and cathode stability [20,23]. Table 3 summarizes the experiments involving improved battery cathodes involved in this paper. As can be seen from the table, the common methods include doping, coating, and reducing the particle size. These methods can increase the discharge capacity by double or even four-times and improve the rate performance of the battery, but this will also bring some problems. For example, the addition of element coatings and the reduction of the particle size may produce by-products, which may lead to cell capacity reduction or pollution [51]. As we all know, doping and coating are not only for the improvement of low-temperature performance, but can optimize the electrochemical performance of the battery as a whole [57–59]. In order to conform to the theme, this paper mainly selected some cases with very significant improvement in low-temperature performance and briefly analyzed the mechanism. Although the examples mentioned in this article also slightly improved the performance of the battery at

room-temperature, the improvement was not obvious compared to the low temperature, as shown in Table 4.

**Table 3.** A summary of tests and results related to cathode materials.

| Cathode                    | Chemistry  | Methods                                 | Action Mechanism   | Test   | Results  | Ref. |
|----------------------------|--|---|--|--|--|------|
| Layered oxides             | 1 M LiPF <sub>6</sub> + EC/PC/EMC, NCM111 CR2025-type coin cells               | Coating Li <sub>3</sub> BO <sub>3</sub> | Li <sub>3</sub> BO <sub>3</sub> coating can reduce the direct contact between the active substance and the electrolyte and can effectively reduce the charge-transfer resistance at low temperatures           | −40 °C, 0.2 C, 2 to 4.8 V, discharge capacity test   | The discharge capacity increased by 173.9%   | [67] |
|                            | 1 M LiPF <sub>6</sub> + DMC/EC (1:1 wt), NCM111 CR2025-type coin cells         | Coating AlF <sub>3</sub>                | The spinel structure produced by aluminum fluoride coating improves ion migration and enhances lithium diffusion kinetics  | −20 °C, 0.1 C, 2.5 to 4.5 V, discharge capacity test | The discharge capacity increased by about 100%   | [60] |
|                            | 1 M LiPF <sub>6</sub> + DMC/EC (1:1 vol), NCM111 2032 coin-type half-cells     | Reducing the particle size              | The layered nanorods assembled with a small particle size have a stable structure, fast ion transport, a large surface area, full contact between the electrolyte and cathode, and good capacity reversibility | 0 °C, 1 C, 3 to 4.4 V, discharge capacity test       | The discharge capacity of the minimum particle size is 27.6% higher than that of the maximum particle size | [61] |
|                            | 1 M LiPF <sub>6</sub> + EMC/DMC/EC (1:1:1 vol) Li/NCM111 R2032-type coin cells | Doping Ti                               | Ti doping can change the lattice parameters of cathodes during charging and discharging and reduce impedance   | −20 °C, 1 C, 2.8 to 4.25 V, discharge capacity test  | The discharge capacity increased by 16.0%  | [68] |
| Spinel-structured oxides   | 1 M LiPF <sub>6</sub> + EC/DEC (3:7 vol), Li/LNMO CR2032-type coin cells       | Coating LATP                            | LATP coating can reduce polarization and charge-transfer resistance at low temperatures, which is conducive to lithium-ion diffusion   | −20 °C, 0.1 C, 3.5 to 5 V, discharge capacity test   | The discharge capacity increased by 71.0%  | [62] |
|                            | Li/LMO coin cells  | Doping Ni                               | Ni doping and the change in the ratio of Mn <sup>4+</sup> –O <sup>2-</sup> bond reduces the energy barrier during charge-transfer by about 20%, alleviating the energy loss at lower temperatures              | −20 °C, 0.2 C capacity retention rate test           | The capacity retention rate increased by 38.5%   | [63] |
| Polyanionic type compounds | 1 M LiPF <sub>6</sub> + EC/DEC (1:1 vol), Li/LFP 2032-type coin cells          | Doping La and Mg                        | Cationic defects caused by doping elements can increase the conductivity, and the porous structure formed by doping shorts the solid-state diffusion path  | −20 °C, 10 C, 2.5 to 4.2 V, discharge capacity test  | The discharge capacity increased by 379.8%   | [64] |

**Table 3.** Cont.

| Cathode | Chemistry  | Methods                | Action Mechanism   | Test   | Results                                   | Ref. |
|---------|--|------------------------|--|--|---|------|
|         | 1 M LiPF <sub>6</sub> + EMC/DMC/EC (1:1:1 vol), LFP 2025-type coin cells | Coating C and doping P | C coating and P doping can alleviate the corrosion of the electrolyte on the cathode and can also establish a certain number of interconnecting channels to shorten the diffusion path of lithium-ions | −25 °C, 1.5 C, 2.7 to 4.2 V, discharge capacity test | The discharge capacity increased by 35.0% | [76] |

**Table 4.** Comparison of the improvement effect of doping and coating methods at low temperature and room-temperature.

| Cathode                    | Chemistry  | Methods                                 | Test  | Results at Low Temperatures                    | Results at Higher Temperatures  | Ref. |
|----------------------------|--|---|---|--|---|------|
| Layered oxides             | 1 M LiPF <sub>6</sub> + EC/PC/EMC, NCM111 CR2025-type coin cells               | Coating Li <sub>3</sub> BO <sub>3</sub> | −40 °C, 20 °C, 0.2 C, 2 to 4.5 V, discharge capacity test   | The discharge capacity increased by 173.9%     | The discharge capacity increased by 6.3%  | [67] |
|                            | 1 M LiPF <sub>6</sub> + DMC/EC (1:1 wt), NCM111 CR2025-type coin cells         | Coating AlF <sub>3</sub>                | −20 °C, 25 °C, 0.1 C, 2.5 to 4.5 V, discharge capacity test | The discharge capacity increased by about 100% | The discharge capacity increased by 4.5%  | [60] |
|                            | 1 M LiPF <sub>6</sub> + EMC/DMC/EC (1:1:1 vol) Li/NCM111 R2032-type coin cells | Doping Ti                               | −20 °C, 25 °C, 1 C, 2.8 to 4.25 V, discharge capacity test  | The discharge capacity increased by 16.0%      | Little improvement  | [68] |
| Spinel-structured oxides   | 1 M LiPF <sub>6</sub> + EC/DEC (3:7 vol), Li/LNMO CR2032-type coin cells       | Coating LATP                            | −20 °C, 25 °C, 0.1 C, 3.5 to 5 V, discharge capacity test   | The discharge capacity increased by 71.0%      | The discharge capacity increased by 6.4%  | [62] |
|                            | Li/LMO coin cells  | Doping Ni                               | −20 °C, 25 °C, 0.2 C capacity retention rate test           | The capacity retention rate increased by 38.5% | Little improvement  | [63] |
| Polyanionic-type compounds | 1 M LiPF <sub>6</sub> + EC/DEC (1:1 vol), Li/LFP 2032-type coin cells          | Doping La and Mg                        | −20 °C, 20 °C, 10 C, 2.5 to 4.2 V, discharge capacity test  | The discharge capacity increased by 379.8%     | The capacity is not mentioned, but the charge-transfer resistance is only about 30Ω higher than at −20 °C | [64] |
|                            | 1 M LiPF <sub>6</sub> + EMC/DMC/EC (1:1:1 vol), LFP 2025-type coin cells       | Coating C and doping P                  | −25 °C, 0 °C, 1.5 C, 2.7 to 4.2 V, discharge capacity test  | The discharge capacity increased by 35.0%      | The discharge capacity increased by 15.0%   | [76] |

From the discussion in this section, we can find that the improvement effect of various schemes on different cathode materials is different on the whole. For layered oxides and spinel-structured oxides, coating is a much more-effective method than doping and particle size reduction, while for polyanionic-type compounds, the opposite is true; doping elements are far more-effective than coating. In summary, the problem of enhancing the low-temperature properties of LIBs using their cathodes needs further study; different methods should be

selected according to the cathode materials of different cathodes; new methods or materials should be explored.

### 3.3. Electrolytes

As seen in the Introduction, at low temperatures, high electrolyte viscosity, high charge-transfer resistance, and severe lithium plating on the anode considerably affect cell performance [20], so new electrolytes should be studied and designed to enable LIBs to work well at low temperatures. Figures 7 and 8 show the effect of optimizing the electrolyte on the low-temperature performance of the battery.

**Aqueous electrolytes.** The advantages of aqueous electrolytes include excellent safety, low cost, lack of environmental pollution, and high ionic conductivity [84,85]. However, pure water generally solidifies at 0 °C, which is unfavorable for battery use at low temperatures [37]. To overcome this defect, Ramanujapuram et al. [86] added 16 mol kg<sup>-1</sup> LiCl, 9 mol kg<sup>-1</sup> LiNO<sub>3</sub>, and 3.5 mol kg<sup>-1</sup> Li<sub>2</sub>SO<sub>4</sub> to water to reduce the freezing point of the solution to −40 °C to 50 °C, −20 °C to 30 °C, and −30 °C to 35 °C, respectively. The capacity retention rate of the cell with LiCl at −40 °C was 72% of that at room-temperature; thus, LiCl is more dominant than conventional organic electrolytes. In addition to this, the researchers established electrochemical impedance spectroscopy (EIS) to study the effect of electrolyte resistance. Figure 8A [86] shows the EIS model used to fit the data. To eliminate the effect of external resistance, plot the X-intercept of the impedance curve as a function of distance, as shown in Figure 8E [86]. The slope of the line in the figure gives the resistivity of the electrolyte per unit length, and plot a function of temperature, as shown in Figure 8F [86]. The true electrolyte resistance is then obtained by repeating the test for each electrolyte at each temperature. Figure 8B–D [86] compares the electrolyte resistance, surface layer resistance, and charge-transfer resistance between −40 °C and 25 °C. The results showed that the increase of the three resistances was not obvious at −35 °C and the increase of the three resistances was sharp at −40 °C, while the increase of the charge-transfer resistance was the largest [86].

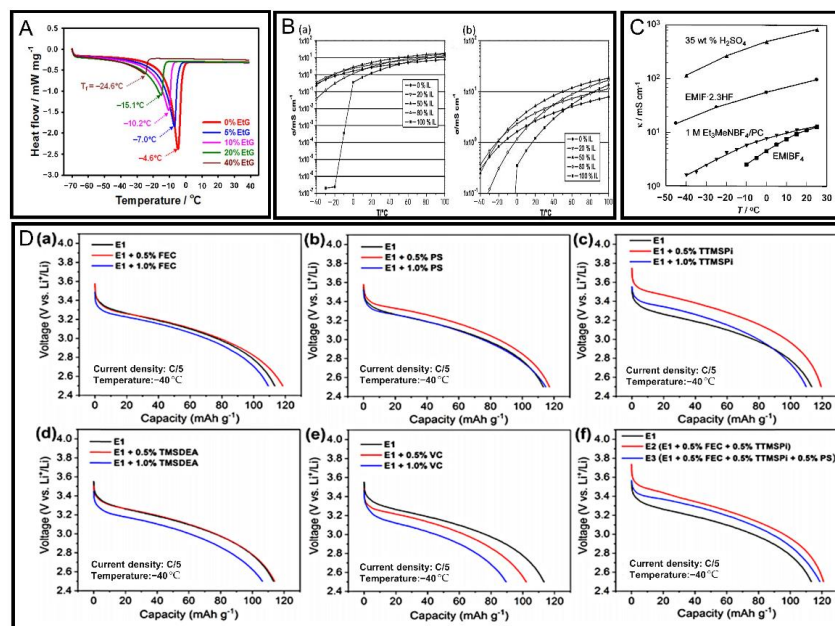


**Figure 7.** Electrolyte design and development. (A) Differential scanning calorimeter analysis of aqueous electrolyte solution containing different amounts of antifreeze additives (EtG, wt%) [87]. (B) Different temperature behaviors of PC-based and PYR14TFSI-based electrolytes. (a) Conductivity of propylene carbonate (PC)-PYR14TFSI-0.3 M LiTFSI ternary mixture with temperature (b) Zoomed-in illustration of high-conductivity region [88]. (C) Variation in the conductivity of various electrolytes with temperature [89]. (D) Influence of different additives on voltage distribution of Gr/NCA battery at −40 °C and 0.2 C [90]. (a) FEC additive, (b) PS additive, (c) TTMSPi additive, (d) TMSDEA additive, (e) VC additive, (f) multiple additives.

In addition, adding antifreeze additives to aqueous electrolytes can prevent solvent crystallization. EtG is widely used in the automobile, electronics, military, aviation, and many other fields because of its low freezing point. Figure 9 [87] shows the action mechanism of EtG in a 1 M Li<sub>2</sub>SO<sub>4</sub> aqueous electrolyte solution. Artur et al. [87] studied aqueous rechargeable lithium-ion batteries (ARLBs) with LFP cathodes without and with different amounts of EtG in 1 M Li<sub>2</sub>SO<sub>4</sub> aqueous electrolyte solutions. The results showed that the crystallization temperature of the electrolyte solution decreased from −4.6 °C to −24.6 °C with the addition of different amounts of EtG (Figure 7A [87]), which greatly improved the low-temperature working range of the ARLBs [87].

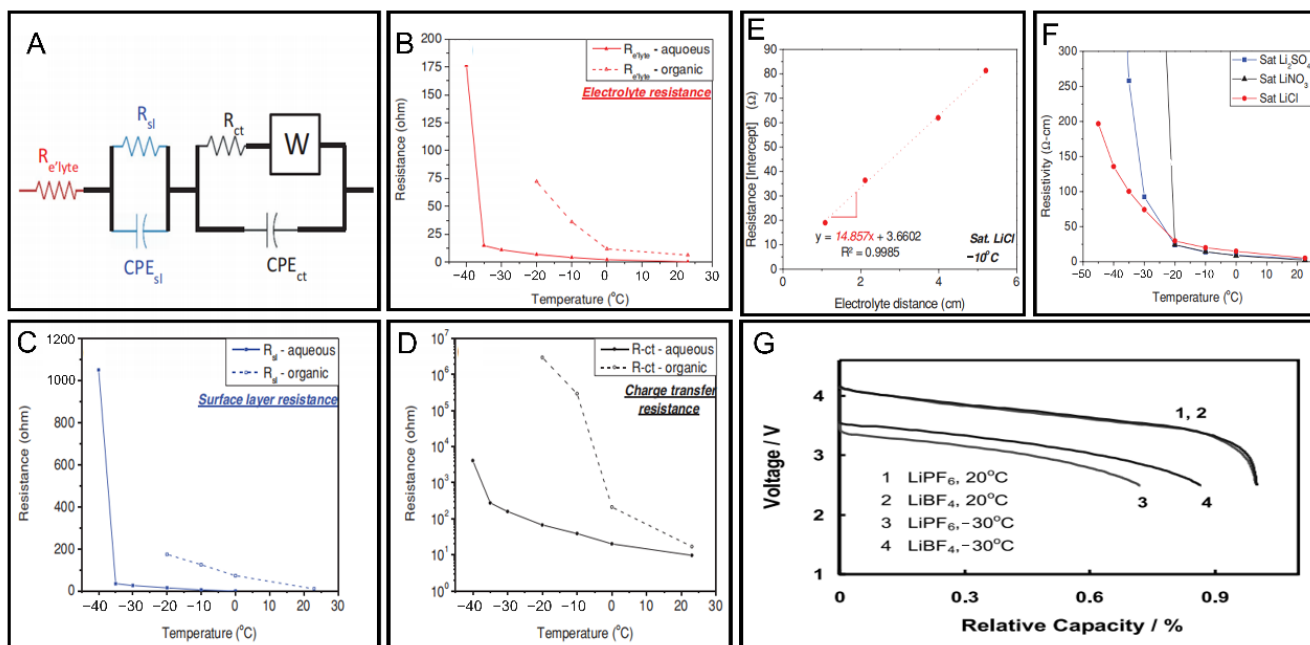


**Figure 8.** Effect of low temperature on electrolyte resistance and enhancement of battery capacity with LiBF<sub>4</sub> electrolyte. (A) Equivalent circuit of aqueous LCO system [86]. (B–D) Comparison of electrolytes, electrolyte surface layers, and charge-transfer resistance with temperature in aqueous and organic electrolyte systems (1 M LiPF<sub>6</sub> in 1:1 EC: DEC) [86]. (E) Relation between X-intercept of impedance curve and electrolyte distance [86]. (F) Comparison of resistivity and temperature of three electrolytes [86]. (G) Influence of different electrolytes on voltage capacity of lithium-ion batteries [91].

**Solid electrolytes.** All-solid-state cells can improve the safety of LIBs, but have poor capacity at low temperatures [20,92,93]. Lin et al. [94] designed a solid electrolyte made of γ-(2,3-epoxypropoxy) propyltrimethoxysilane and boron (B) materials co-cross-linked with starch (B-starch-Si (BStSi)) [20,94]. The Li/LFP battery with BStSi electrolyte was placed in the refrigerator (Haier, BCD-220WDVL), and the battery's performance was tested in the battery test system (LAND CT2001A, BTRBTS) under an anti-static charge-discharge cycle at −20 °C. After 200 cycles at −20 °C, the capacity of the Li/LFP cell containing this electrolyte reached 55.9 mAh g<sup>−1</sup>, which was 46.5% of its room-temperature capacity. This greatly enhanced the performance of the lithium battery at low temperatures and extended the working time of the battery [94]. Li et al. [95] designed and synthesized a covalent organic frameworks (COFs) solid electrolyte; after lithiation, the COFs were stripped to form covalent organic nanosheets, which promoted single-ion conduction without a solvent. Consequently, it quickly combined with and separated from the lithium-ions, thereby greatly enhancing ionic conductivity (10<sup>−5</sup> S/cm at −40 °C) [95].

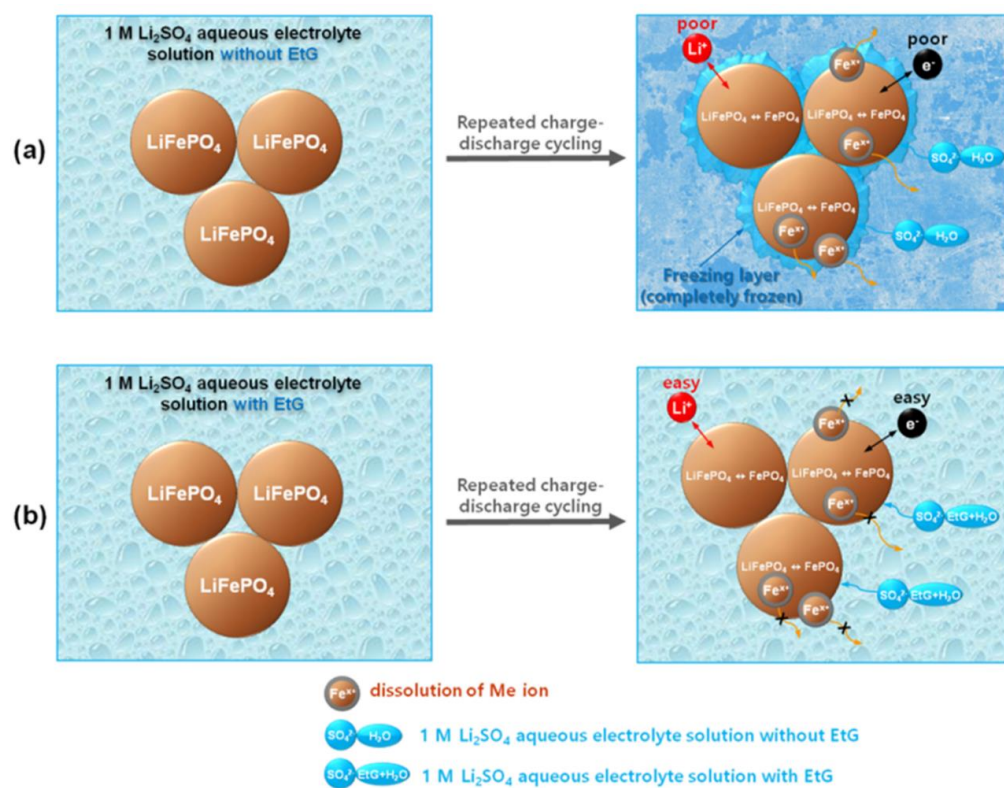


**Figure 9.** Schematic diagram of LFP material particles in 1 M  $\text{Li}_2\text{SO}_4$  hydrolylate solutions (a,b) [87].

**Cryogenic ionic liquid electrolytes.** Ionic liquids have a wide working temperature range and can enhance the low-temperature characteristic of LIBs [20,96–98]. bis(trifluoromethanesulfonyl)imide (TFSI)-based ionic liquids exhibit good, stable electrochemical performance [20]. Aguilera et al. [99] introduced N-butyl-N-methylpyrrolidinium (PYR14)-TFSI into a traditional electrolyte; its freezing point was lower than that of a carbonate-based electrolyte, and it enhanced the low-temperature performance of the cell. Ionic liquids are attracting extensive attention because of their wide electrochemical window and remarkable safety [100]. In the study of Balducci et al. [88], the ionic liquid N-butyl-N-methylpyrrolidiniumbis(trifluoromethanesulfonyl)imide (PYR14TFSI) and propylene carbonate (PC) were mixed in different proportions to form electrolytes with various conductivities at different temperatures. Conductivity is measured using a slave-phase-controlled Alpha analyzer and a slave-phase-controlled temperature controller. Figure 7B [88] shows that the conductivity of an electrolyte with 20% and 50% PYR14TFSI added at  $-30^\circ\text{C}$  to  $0^\circ\text{C}$  was higher than that of an electrolyte without PYR14TFSI; moreover, the conductivity of the 20% group decreased more slowly with the decrease in temperature. It can be shown that the addition of 20% PYR14tfsi prevented the electrolyte from freezing, at least up to  $-40^\circ\text{C}$  [88]. Makoto et al. [89] used the ionic liquid 1-ethyl-3-methylimidazolium fluoride (EMIF)·2.3 HF as an electrolyte, and the conductivities of electrolytes were measured by a conductivity meter (Toa Electronics, CM-50S/CGT-511B). The results showed that the conductivity of their capacitor reached  $20 \text{ mS cm}^{-1}$  at  $-40^\circ\text{C}$ , which was better than that of a non-aqueous electrolyte (1 M  $\text{Et}_3\text{MeNBF}_4$ /PC) (Figure 7C [89]). Although some ionic liquid electrolytes are challenging to obtain, they play an important role in the development of low-temperature LIBs.

**Organic electrolytes.** Organic electrolytes are the most-traditional LIB electrolytes. Solvents, lithium salts, and additives generally need to be adjusted to prepare organic electrolytes [101–103]. Therefore, enhancing the low-temperature properties of cells from the perspective of organic electrolytes should begin with these three aspects.

In terms of the solvent, low-melting-point cosolvents can be incorporated to improve the low-temperature properties of LIBs. Dong et al. [37,104] used a high-concentration

electrolyte composed of 5 M LiTFSI, a dichloromethane (DCM) diluent, and an ethyl acetate (EA) electrolyte. The experimental data showed that the electrolyte had high ionic conductivity ( $0.6 \text{ mS cm}^{-1}$ ) at  $-70^\circ\text{C}$ . As for lithium salts, and the anion modification of lithium salts may provide more lithium-ions to the electrolytes and improve ionic mobility [105]. Compared with traditional LiPF<sub>6</sub>-based carbonate electrolytes, LiBF<sub>4</sub>-, LiBOB-, and LiDFOB-based carbonate electrolytes can improve ionic mobility, thus enhancing the low-temperature working ability of LIBs [106]. In particular, the LiBF<sub>4</sub>-based electrolyte has a better working ability at low temperatures. Zhang et al. [91] prepared 1 M LiBF<sub>6</sub> and 1 M LiBF<sub>4</sub> electrolytes in a glovebox filled with argon gas and dissolved them in 1:1:3 PC/EC/EMC solvent to study the low-temperature performance of batteries with a graphite anode and lithium nickel-based mixed oxide cathode. Figure 8G [91] compares the cell polarization caused by the use of different electrolytes. As can be seen from the figure, the volt–capacity curves of LiBF<sub>6</sub> and LiBF<sub>4</sub> batteries were very close at  $20^\circ\text{C}$ , but interestingly, the capacity of batteries containing LiBF<sub>4</sub> had a relatively significant increase at  $-30^\circ\text{C}$ , which indicates that LiBF<sub>4</sub> plays a good role in improving the low-temperature performance of LIBs [91]. In addition to solvents and lithium salts, additives can remarkably enhance the low-temperature working ability of LIBs from the perspective of organic electrolytes. Additives can form stable SEIs, change the SEI composition, decrease the charge-transfer resistance, contribute to the uniform deposition of Li, and inhibit the growth of Li dendrites [105]; these additives include FEC, 1,3-propanesultane, and tris(trimethylsilyl) phosphor (TMSP). In addition, when lithium-silica sulfobetaine silane and hydroxyl-terminated poly(dimethylsiloxane) are mixed in a certain way, the synergistic effect between them can enhance the conductivity of the battery. This material can enhance the low-temperature properties of LIBs and is also a promising carbonate-based electrolyte additive [107]. Liu et al. [90] compared electrolytes E1 (0.05 M CsPF<sub>6</sub> containing 1 M LiPF<sub>6</sub> + PC/ethyl methyl carbonate (EMC)/ethylene carbonate (EC) [1:8:1 wt]), E2, and E3, which contained different additives (Figure 7D [90]), to study the influence of the additive type and concentration on the low-temperature working ability of a GR/LiNi<sub>0.08</sub>Co<sub>0.15</sub>Al<sub>0.05</sub>O<sub>2</sub> (Gr/NCA) button cell. The cell with 0.5% of the electrolyte additive exhibited better discharge performance at  $-40^\circ\text{C}$  (Figure 7D(a–e) [90]). The batteries containing E2 and E3 had better low-temperature performance, with the E2 electrolyte showing better performance (Figure 7D(f) [90]). Gao et al. [108] designed a 1 M LiPF<sub>6</sub> + methyl acetate (MA)/EMC/EC/diethyl carbonate (DEC) (3:1:1:1 vol; baseline electrolyte (BE) + MA) electrolyte. They incorporated 1 wt% TMSP + 1 wt% 1,3-propanediolic sulfate (PCS) as an additive, and the resulting electrolyte was named BE + MA + TMSP + PCS. In the experiment, they used the LAND System (CT2001A, Wuhan, China) to charge and discharge LiNi<sub>0.5</sub>Mn<sub>1.5</sub>O<sub>4</sub>/MCMB full cells at different temperatures, and the current was calculated from the LiNi<sub>0.5</sub>Mn<sub>1.5</sub>O<sub>4</sub> cathode material (1 C rate set to  $120 \text{ mA g}^{-1}$ ). Then, they evaluated the low-temperature properties of a graphitic mesocarbon microbead (MCMB)/LNMO cell and concluded that the capacity retention rate of the cell with BE + MA + TMSP + PCS was 99.7% ( $101.7 \text{ mAh g}^{-1}/102 \text{ mAh g}^{-1}$ ) at a charge–discharge rate of 0.3 C at  $-5^\circ\text{C}$ . This showed that the battery using the BE + MA + TMSP + PCS electrolyte had better performance at low temperature [108]. The abovementioned FEC additives have been studied extensively. He et al. [109] tested the influence of FEC additives on the ionic conductivity of Li/lithium cobalt acid cells at  $-40^\circ\text{C}$  to  $25^\circ\text{C}$ . At  $-40^\circ\text{C}$ , and the conductivities of electrolytes without FEC and with 5, 10, and 20 wt% FEC electrolytes were  $5.42 \times 10^{-4}$ ,  $1.55 \times 10^{-3}$ ,  $2.35 \times 10^{-3}$ , and  $1.63 \times 10^{-3} \text{ S cm}^{-1}$ , respectively. At room-temperature, the ionic conductivities of electrolytes were  $1.11 \times 10^{-2}$ ,  $8.55 \times 10^{-3}$ ,  $8.86 \times 10^{-3}$ , and  $1.42 \times 10^{-2} \text{ S cm}^{-1}$ , respectively. The electrolyte with 10 wt% FEC showed the maximum conductivity at both low and room-temperatures. The conductivities of the electrolytes without FEC decreased rapidly with a decrease in temperature. Adding an appropriate amount of the FEC additive (according to the experimental data, approximately 10 wt% FEC had the best effect) helped improve the ionic conductivity, and the lower the temperature, the more obvious the effect was. The researchers [109] also tested the effect of different

concentrations of FEC additives on the battery discharge capacity. The experimental results showed that the capacity retention rate of the battery without the FEC additive was 66% and that of the cell having 10 wt% FEC was 77.1% at  $-40^{\circ}\text{C}$  and 0.2 C. The addition of FEC benefited the low-temperature performance of the battery. Their experimental results showed that the capacity retention rate of the battery with 10 wt% FEC was greater than not only that of the battery without the FEC additive, but also that of the battery with 20% FEC. Therefore, the FEC additive improved the low-temperature properties of the cells, but a higher FEC concentration did not lead to better battery performance [109]. In short, the design of electrolytes, including aqueous electrolytes, solid electrolytes, ionic liquid electrolytes, and organic electrolytes, has a considerable improvement in the discharge capacity of lithium-ion batteries at low temperatures and greatly extends the use time of batteries at low temperatures.

Table 5 summarizes the experiments mentioned in this paper to improve the low-temperature performance of LIBs from the perspective of the electrolyte. The data in the table show that improving the electrolyte is very helpful to enhance the ionic conductivity and can even increase the ionic conductivity by more than 60-times.

**Table 5.** A summary of tests and results related to different electrolytes.

| Electrolyte                        | Chemistry   | Methods                            | Test   | Results   | Ref.  |
|------------------------------------|---|------------------------------------|--|---|-------|
| Aqueous electrolyte                | saturated LiCl aqueous electrolyte solutions, LiCoO <sub>2</sub> cells    | Adding inorganic salt              | $-40^{\circ}\text{C}$ , 0.2 C, capacity retention rate test  | Without improvement: cannot work<br>After improvement: capacity retention rate is 72%                         | [86]  |
|                                    | 1 M Li <sub>2</sub> SO <sub>4</sub> aqueous electrolyte solutions         | Adding EtG                         | Cooling/heating rate: $5^{\circ}\text{C min}^{-1}$<br>$40^{\circ}\text{C}$ to $-70^{\circ}\text{C}$ , differential scanning calorimeter analysis | The crystallization temperature is reduced to $-20^{\circ}\text{C}$   | [87]  |
| Cryogenic ionic liquid electrolyte | PYR14TFSI ionic liquid electrolyte, LFP cells                             | mixing PC                          | $-20^{\circ}\text{C}$ , conductivity test  | The conductivity is increased by more than $10^6$ times   | [88]  |
|                                    | EMIF-2.3 HF ionic liquid electrolyte, 2032-type coin cells                | Ionic liquid EMIF-2.3 HF           | $-40^{\circ}\text{C}$ , conductivity test  | The conductivity is about 10-times higher than that of 1 M Et <sub>3</sub> MeNBF <sub>4</sub> /PC electrolyte | [89]  |
| Organic electrolyte                | 5 M LiTFSI/EA + DCM (1:4 vol), Li/P cells                                 | Adding low melting point cosolvent | $-70^{\circ}\text{C}$ , conductivity test  | The conductivity is 60-times higher than that of ordinary carbonate-based electrolyte                         | [104] |
|                                    | 1 M LiPF <sub>6</sub> + MA/DEC/EC/EMC (3:1:1:1 vol), MCMB/LNMO full-cells | Adding TMSP and PCS additive       | $-5^{\circ}\text{C}$ , 0.3 C, 3.5 V to 4.9 V, capacity retention rate test   | The capacity retention rate increased by 34.2%  | [108] |
|                                    | 1 M LiPF <sub>6</sub> + EP/EMC/EC (4:1:1 wt), Li/LiCoO <sub>2</sub> cells | Adding FEC additive                | $-40^{\circ}\text{C}$ , ionic conductivity test  | The ionic conductivity increased by 333.6%  | [109] |
|                                    | 1 M LiPF <sub>6</sub> + EP/EMC/EC (4:1:1 wt), Li/LiCoO <sub>2</sub> cells | Adding FEC additive                | $-40^{\circ}\text{C}$ , 0.2 C, 3.0 V to 4.2 V, capacity retention rate test  | The capacity retention rate increased by 16.8%  | [109] |

In general, researchers have used different methods to examine various types of electrolytes, but they all aim to improve the low-temperature properties of LIBs by reducing

the freezing point of electrolytes, improving their ionic conductivity and improving their chemical properties, among others. The research process is hampered by many questions and difficulties, such as the selection of additives, the selection of additive volumes, and whether such added substances harm the environment. In addition, reducing additives may undergo oxidation reactions on the cathode, whereas FEC additives form thick SEI films on the graphite electrodes of PC and EC electrolyte systems [110]. All in all, the design and study of electrolytes at low temperatures need to be further pursued.

#### 4. The Advantages and Disadvantages of Different Schemes

Each of the methods above has its advantages, but often comes with disadvantages. As shown in Table 6, for example, pre-lithiation treatment can improve battery capacity and energy density, but it cannot increase ionic conductivity. What is more, adding additives in electrolyte can enhance the electrochemical performance of the electrolyte at low temperatures, but some reducing additives undergo an oxidation reaction at the cathode, which is bad for LIBs. In order to obtain a better comprehensive performance of LIBs, it is suggested that material optimization should be combined with structure optimization. For example, a low-melting-point cosolvent can be added to the electrolyte at the same time as the anode material is prelithiated. This can not only inhibit the occurrence of lithium-plating in LIBs at low temperatures, but also improve the ionic conductivity.

**Table 6.** The advantages and disadvantages of different schemes.

| Scheme                                  | Perspective    | Concrete Measures  | Advantage  | Disadvantage  | Ref.    |
|---|----------------|--|--|---|---------|
| Cell fabrication/structure optimization | Low tortuosity | 3D printing  | Improves lithium-ion transport efficiency<br>Increases cycle life<br>Reduces electrode tortuosity  | Cannot be used easily for large-scale industrial manufacturing  | [30]    |
|   |                | Use of new composite separator                                     | Significantly increases lithium-ion transference number and lithium-ion conductivity<br>Reduces interface resistance between electrolyte and electrode<br>Significantly improves rate performance and cycle durability | Not mentioned   | [31]    |
| Electrode materials                     | Anode          | Removal of solvent components from electrode                       | Improves ionic transport efficiency in electrode<br>Has low cost   | Increases electrode tortuosity  | [28]    |
|   |                | Introduction of orderly directional pore structures into electrode | Effectively reduces tortuosity of electrode structure<br>Improves hole regularity<br>Improves lithium-ion transport efficiency   | Has high complexity<br>Needs more methods of directional introduction of holes  | [28–32] |
|   |                | Pre-lithiation treatment   | Alleviates lithium plating   | Cannot increase ionic conductivity<br>Affects improvement effect of pre-lithiation through low ionic conductivity of electrolytes at low temperatures | [38]    |

**Table 6.** Cont.

| Scheme               | Perspective                         | Concrete Measures  | Advantage  | Disadvantage   | Ref.       |
|----------------------|-------------------------------------|--|--|--|------------|
| Cathode              | Element doping                      | Element doping   | Increases battery capacity<br>Improves rate capacity and cycle stability   | May negatively affect battery capacity at room-temperature   | [40–42]    |
|                      |                                     | Particle size reduction  | Effectively reduces transport paths of ions and electrons<br>Improves solid diffusion kinetics                         | May cause side effects due to increased surface area   | [49,77]    |
|                      |                                     | Development of next generation of negative electrode materials, such as Si | Has high theoretical capacity, low possibility of lithium plating, good safety, and low cost (Si)                      | Leads to severe volume expansion   | [43,50,51] |
|                      | Addition of coatings                | Addition of coatings   | Protects cathode surface from liquid electrolytes and unwanted side reactions<br>Reduces battery polarization          | May hinder lithium-ion transport due to thick coating, affecting storage of lithium-ions                       | [60,67]    |
|                      |                                     | Particle size reduction  | Same as those for anode materials  |  |            |
|                      |                                     | Element doping   | Same as those for anode materials  |  |            |
|                      | Aqueous electrolytes                | Addition of inorganic salt   | Reduces freezing point of solution<br>Improves performance at low temperatures   | Not mentioned  | [86]       |
|                      |                                     | Addition of antifreeze   | Prevents solution crystallization  | May easily generate acidic substances, corroding metal   | [37,96]    |
|                      | Solid electrolytes                  | Use of starch-based solid electrolyte                                      | Improves transport ability of lithium-ions and working performance of LIBs at low temperatures and high pressures      | Requires difficult electrolyte preparation<br>Has high cost  | [94]       |
|                      |                                     | Use of COF solid electrolyte   | Promotes single-ion conduction<br>Rapidly combines with and separates from lithium-ions<br>Improves ionic conductivity | Has high preparation cost<br>Exhibits poor long-term use stability   | [95]       |
|                      |                                     | Mixture of ionic liquid with traditional electrolyte                       | Reduces freezing point of electrolyte<br>Improves low-temperature performance of battery                               | Not mentioned  | [99,100]   |
| Electrolytes         | Cryogenic ionic liquid electrolytes | Addition of low-melting-point cosolvent                                    | Improves ionic conductivity at low temperatures  | Can easily cause environmental pollution due to chemical composition   | [37,104]   |
|                      |                                     | Lithium salt anion modification  | Improves ionic mobility  | May decrease electrolyte conductivity due to low solubility of some modified lithium salts in aprotic solvents | [105]      |
| Organic electrolytes |                                     |  |  |  |            |

**Table 6.** Cont.

| Scheme | Perspective           | Concrete Measures                                   | Advantage   | Disadvantage | Ref. |
|--------|-----------------------|---|---|--------------|------|
|        | Addition of additives | Improves electrochemical performance of electrolyte | May cause oxidation reaction on cathode (for some reducing additives)<br>Increases difficulty of determining additive amount<br>May cause graphite electrode to form thick SEI film (for certain electrolyte additives) | [107,109]    |      |

## 5. Summary and Outlook

This review presented the current research status of the methods of enhancing the low-temperature performance of LIBs at the cell design level. The low-temperature applications of LIBs here point to electric vehicles. First, the article highlighted the necessity of the development of new-energy vehicles and the benefits of LIBs as a power supply for new-energy vehicles from two current situations: the increasing demand for energy resources and the increasingly prominent environmental problems worldwide [1–3]. Low temperatures are then emphasized as an important factor limiting the use of new-energy vehicles. Next, this review introduced the deterioration of the low-temperature performance of LIBs and pointed out the main parameters to control or improve the performance of LIBs at low temperatures. Then, this review summarized four factors that deteriorate the performance of LIBs at low temperatures, which are the decreased ionic conductivity and wettability of liquid electrolytes, the increased intrinsic grain-boundary resistance and slow Li<sup>+</sup> diffusion rate in electrodes, and the difficult Li<sup>+</sup> dissolution and sluggish Li<sup>+</sup> transport through solid-electrolyte interphase (SEI) along with high charge-transfer resistance and the occurrence of Li plating [20], and explained what consequences these factors will lead to. Moreover, this paper illustrated the key consideration to improve the deteriorated capacity, so that readers can understand how to enhance the low-temperature performance of cells clearly. In addition, this paper summarized the methods to enhance the low-temperature performance of LIBs from two aspects and put forward the idea that the two should be combined.

Thus, several common methods of improving the low-temperature properties of cells were introduced in detail from the viewpoint of cell design. Methods to enhance the performance of the cell by optimizing the cell structure were introduced first. For example, electrodes with high porosity and low tortuosity can improve the transport efficiency of lithium-ions at low temperatures [23]. Electrode materials were then discussed. The effects of anode, cathode, and electrolyte materials on the low-temperature properties of LIBs were analyzed in detail. The common improvement methods of cathode and anode materials mainly include doping, coating, and particle size reduction. Coatings generally protect the cathode from corrosion, reduce polarization, and increase capacity, while doping elements can change the lattice parameters or chemical bonds of the cathode to slow the rate of increase of charge-transfer resistance at sub-zero temperatures. Reducing the particle size can increase the surface area of the electrode and shorten the diffusion path of lithium-ions [56–59]. Here, the effects of these three methods on different anode and cathode materials were explained using examples, and the problems faced by these materials and methods, such as possible side reactions, were also highlighted. This review also discussed the most-common organic electrolytes, which can be improved by developing low-melting-point cosolvents, exploring new lithium salts, and studying various low-temperature additives. Moreover, the advantages of aqueous, solid, and ionic liquid electrolytes, along with their optimization methods for low-temperature applications were also discussed.

In general, from the perspective of cell design, the methods of improving the low-temperature properties of LIBs include battery structure optimization, electrode optimization, electrolyte material optimization, etc. These can increase the reaction kinetics and the upper limit of the working capacity of cells. An electrolyte with a low freezing point, which can form a stable SEI with low impedance, needs to be developed. In addition, electrode optimization for high ionic conductivity, high energy density, and lithium plating prevention is a research hotspot [23]. Future studies can also focus on using various materials to induce synergistic effects for the improvement of cell materials.

Leaving aside the single point of view of battery design, future research should also combine battery management with battery materials to fully achieve the enhancement potential of the low-temperature properties of LIBs. The thermal management system can improve the working environment of the battery at low temperatures, such as air preheating [111], resistance preheating [112], phase change material preheating [113], self-heating techniques [114], and current excitation techniques [115]. Researchers have explored methods of enhancing the low-temperature properties of LIBs, but they only focus on a certain topic, and few scholars have proposed systematic solutions to the abovementioned problems. Combining material optimization schemes from the intrinsic aspect of batteries with thermal management schemes for an improved battery environment may result in a breakthrough in the low-temperature performance of batteries.

**Author Contributions:** Conceptualization, J.Z., W.L. and Z.G.; methodology, J.Z. and Y.D.; software, J.Z. and J.R.; validation, J.Z., J.R. and Y.G.; formal analysis, J.Z. and S.R.; investigation, J.Z., Y.D., J.R., Y.G. and Y.L.; resources, J.Z., W.L. and Z.G., writing—original draft preparation, J.Z., Y.D., J.R., Y.G. and Y.L.; writing—review and editing, W.L., Z.G. and J.Z., visualization, J.Z., Y.G. and S.R.; funding acquisition, W.L. and Z.G. All authors have read and agreed to the published version of the manuscript.

**Funding:** This research received no external funding.

**Data Availability Statement:** All the data used in this research work are incorporated in the manuscript.

**Acknowledgments:** This research was supported by the Jilin Provincial Science and Technology Development Plan Project (No. 20220508003RC), the National Natural Science Foundation of China (No. 52202440), the Scientific research projects of the Education Department of Jilin Province (JKH20221001KJ), the Open Funds of State Key Laboratory of Automotive Safety and Energy (KFY2224), and the Fundamental Research Funds for the Central Universities (415010300061,2022-JCXB-24).

**Conflicts of Interest:** The authors declare no conflict of interest.

## Abbreviations

The following abbreviations are used in this manuscript:

| Abbreviation | Full form/Chemical Name                    | Abbreviation | Full form/Chemical Name  |
|--------------|--|--------------|--|
| ARLBs        | Aqueous rechargeable lithium-ion batteries | LNCM         | $\text{Li}[\text{Ni}_x\text{Co}_y\text{Mn}_{1-x-y}] \text{O}_2$ ( $0 < x < 1, 0 < y < 1$ ) |
| BE           | Baseline electrolyte                       | LNMO         | $\text{LiNi}_{0.5}\text{Mn}_{1.5}\text{O}_4$   |
| BStSi        | B-starch-Si                                | LP           | 1 M LiPF <sub>6</sub> in ethylene carbonate/diethyl carbonate                              |
| CA           | carbon aerogel                             | LTO          | $\text{Li}_4\text{Ti}_5\text{O}_{12}$  |
| COFs         | Covalent organic frameworks                | LVP          | $\text{Li}_3\text{V}_2(\text{PO}_4)_3$   |
| DCM          | Dichloromethane                            | MA           | Methyl acetate   |
| DEC          | Diethyl carbonate                          | MCMB         | Graphitic mesocarbon microbead   |
| DMC          | Dimethyl carbonate                         | MOF          | Metal–organic framework  |
| EA           | Ethyl acetate                              | NCA          | $\text{LiNi}_{0.80}\text{Co}_{0.15}\text{Al}_{0.05}\text{O}_2$                             |
| EC           | Ethylene carbonate                         | NCM111       | $\text{LiNi}_{1/3}\text{Co}_{1/3}\text{Mn}_{1/3}\text{O}_2$                                |
| EIS          | Electrochemical impedance Spectroscopy     | NCM622       | $\text{LiNi}_{0.6}\text{Co}_{0.2}\text{Mn}_{0.2}\text{O}_2$                                |
| EMC          | Ethyl methyl carbonate                     | PC           | Propylene carbonate  |
| EMIF         | 1-ethyl-3-methylimidazolium Fluoride       | PCS          | 1,3-propanediolic sulfate  |
| EMP          | Electrospun MOF–PVA composite membranes    | PP           | Polypropylene  |

|      |   |           |   |
|------|---|-----------|---|
| EtG  | Ethylene glycol   | PYR14TFSI | N-butyl-N-Methylpyrrolidiniumbis(trifluoromethanesulfonyl)imide |
| FEC  | Fluoroethylene carbonate  | SEAG      | a-Si nano-layer   |
| LATP | $\text{Li}_2\text{O}-\text{Al}_2\text{O}_3-\text{TiO}_2-\text{P}_2\text{O}_5$ | SEI       | Solid-electrolyte interphase                                    |
| LC   | 1 M $\text{LiClO}_4$ in propylene carbonate                                   | SP        | Smaller primary particle size                                   |
| LFP  | $\text{LiFePO}_4$   | TFSI      | Bis(trifluoromethanesulfonyl)imide                              |
| LIBs | Lithium-ion batteries   | TMSP      | Tris(trimethylsilyl) phosphite                                  |
| LMO  | $\text{LiMn}_2\text{O}_4$   |           |   |

## References

- IEA. *World Energy Outlook 2022*; IEA: Paris, France, 2022. Available online: <https://www.iea.org/reports/world-energy-outlook-2022> (accessed on 1 October 2022).
- UNEP. *The Closing Window—Climate Crisis Calls for Rapid Transformation of Societies*; UNEP: Nairobi, Kenya, 2022. Available online: <https://www.unep.org/resources/emissions-gap-report-2022> (accessed on 27 October 2022).
- General Office of the State Council of China. Circular of The General Office of the State Council on Printing and Distributing the Development Plan for the New Energy Automobile Industry (2021–2035). Available online: [http://www.gov.cn/zhengce/content/2020-11/02/content\\_5556716.htm](http://www.gov.cn/zhengce/content/2020-11/02/content_5556716.htm) (accessed on 20 October 2020).
- Xiong, R.; Chen, H.; Wang, C.; Sun, F. Towards a smarter hybrid energy storage system based on battery and ultracapacitor—A critical review on topology and energy management. *J. Clean. Prod.* **2018**, *202*, 1228–1240. [[CrossRef](#)]
- Li, Z.H.; Khajepour, A.; Song, J.C. A comprehensive review of the key technologies for pure electric vehicles. *Energy* **2019**, *182*, 824–839. [[CrossRef](#)]
- Fu, S.J.; Fu, H.J. A method to predict electric vehicles' market penetration as well as its impact on energy saving and  $\text{CO}_2$  mitigation. *Sci. Prog.* **2021**, *104*, 00368504211040286. [[CrossRef](#)]
- Tong, F.; Azevedo, I.M.L. What are the best combinations of fuel-vehicle technologies to mitigate climate change and air pollution effects across the United States? *Environ. Res. Lett.* **2020**, *15*, 074046. [[CrossRef](#)]
- Ashok, B.; Kannan, C.; Mason, B.; Ashok, S.D.; Indragandhi, V.; Patel, D.; Wagh, A.S.; Jain, A.; Kavitha, C. Towards Safer and Smarter Design for Lithium-Ion-Battery-Powered Electric Vehicles: A Comprehensive Review on Control Strategy Architecture of Battery Management System. *Energies* **2022**, *15*, 4227. [[CrossRef](#)]
- Hemavathi, S. Overview of cell balancing methods for Li-ion battery technology. *Energy Storage* **2020**, *3*, e203. [[CrossRef](#)]
- Zubi, G.; Dufo-López, R.; Carvalho, M.; Pasaoglu, G. The lithium-ion battery: State of the art and future perspectives. *Renew. Sustain. Energy Rev.* **2018**, *89*, 292–308. [[CrossRef](#)]
- Dobrzycki, A.; Filipiak, M.; Jajczyk, J. Changes in the range of electric vehicles during operation. In Proceedings of the Conference on Computer Applications in Electrical Engineering (ZkwE), Poznan, Poland, 15 April 2019.
- Xu, J.J.; Cai, X.Y.; Cai, S.M.; Shao, Y.X.; Hu, C.; Lu, S.R.; Ding, S.J. High-Energy Lithium-Ion Batteries: Recent Progress and a Promising Future in Applications. *Energy Environ. Mater.* **2023**. *Epub ahead of print*. [[CrossRef](#)]
- Van Ree, T. Electrolyte additives for improved lithium-ion battery performance and overcharge protection. *Curr. Opin. Electrochem.* **2020**, *21*, 22–30. [[CrossRef](#)]
- Li, Q.Y.; Jiao, S.H.; Luo, L.L.; Ding, M.S.; Zheng, J.M.; Cartmell, S.S.; Wang, C.M.; Xu, K.; Zhang, J.G.; Xu, W. Wide-Temperature Electrolytes for Lithium-Ion Batteries. *ACS Appl. Mater. Interfaces* **2017**, *9*, 18826–18835. [[CrossRef](#)]
- Jaguemont, J.; Boulon, L.; Dube, Y. Low Temperature Discharge Cycle Tests for a Lithium Ion Cell. In Proceedings of the 2014 IEEE Vehicle Power and Propulsion Conference (VPPC), Coimbra, Portugal, 27–30 October 2014.
- Hubble, D.; Brown, D.E.; Zhao, Y.; Fang, C.; Lau, J.; McCloskey, B.D.; Liu, G. Liquid electrolyte development for low-temperature lithium-ion batteries. *Energy Environ. Sci.* **2022**, *15*, 550–578. [[CrossRef](#)]
- Gupta, A.; Manthiram, A. Designing Advanced Lithium-Based Batteries for Low-Temperature Conditions. *Adv. Energy Mater.* **2020**, *10*, 2001972. [[CrossRef](#)] [[PubMed](#)]
- Yoo, D.-J.; Liu, Q.; Cohen, O.; Kim, M.; Persson, K.A.; Zhang, Z. Understanding the Role of SEI Layer in Low-Temperature Performance of Lithium-Ion Batteries. *ACS Appl. Mater. Interfaces* **2022**, *14*, 11910–11918. [[CrossRef](#)] [[PubMed](#)]
- Zhao, D.; Song, L.; Wang, J.; Zhang, J.; Cui, X.; Wang, P.; Sun, J.; Cai, X.; Huang, J.; Zhang, N.; et al. Insight into the competitive reaction between LiDFP and LiFSI in lithium-ion battery at low temperature. *J. Power Sources* **2022**, *549*, 232147. [[CrossRef](#)]
- Zhang, N.; Deng, T.; Zhang, S.; Wang, C.; Chen, L.; Wang, C.; Fan, X. Critical Review on Low-Temperature Li-Ion/Metal Batteries. *Adv. Mater.* **2022**, *34*, 2107899. [[CrossRef](#)]
- Hu, D.; Chen, L.; Tian, J.; Su, Y.; Li, N.; Chen, G.; Hu, Y.; Dou, Y.; Chen, S.; Wu, F. Research Progress of Lithium Plating on Graphite Anode in Lithium-Ion Batteries. *Chin. J. Chem.* **2020**, *39*, 165–173. [[CrossRef](#)]
- Hu, A.; Li, F.; Chen, W.; Lei, T.; Li, Y.; Fan, Y.; He, M.; Wang, F.; Zhou, M.; Hu, Y.; et al. Ion Transport Kinetics in Low-Temperature Lithium Metal Batteries. *Adv. Energy Mater.* **2022**, *12*, 2202432. [[CrossRef](#)]
- Piao, N.; Gao, X.; Yang, H.; Guo, Z.; Hu, G.; Cheng, H.-M.; Li, F. Challenges and development of lithium-ion batteries for low temperature environments. *Etransportation* **2022**, *11*, 100145. [[CrossRef](#)]

24. Zhang, M.; Chouchane, M.; Shojaee, S.A.; Winiarski, B.; Liu, Z.; Li, L.; Pelapur, R.; Shodiev, A.; Yao, W.; Doux, J.-M.; et al. Coupling of multiscale imaging analysis and computational modeling for understanding thick cathode degradation mechanisms. *Joule* **2022**, *7*, 201–220. [CrossRef]
25. Zhou, S.; Huang, P.; Xiong, T.; Yang, F.; Yang, H.; Huang, Y.; Li, D.; Deng, J.; Balogun, M.J.T. Sub-Thick Electrodes with Enhanced Transport Kinetics via In Situ Epitaxial Heterogeneous Interfaces for High Areal-Capacity Lithium Ion Batteries. *Small* **2021**, *17*, e2100778. [CrossRef]
26. Wang, N.; Zhang, X.; Ju, Z.; Yu, X.; Wang, Y.; Du, Y.; Bai, Z.; Dou, S.; Yu, G. Thickness-independent scalable high-performance Li-S batteries with high areal sulfur loading via electron-enriched carbon framework. *Nat. Commun.* **2021**, *12*, 4519. [CrossRef] [PubMed]
27. He, R.; Tian, G.; Li, S.; Han, Z.; Zhong, W.; Cheng, S.; Xie, J. Enhancing the Reversibility of Lithium Cobalt Oxide Phase Transition in Thick Electrode via Low Tortuosity Design. *Nano Lett.* **2022**, *22*, 2429–2436. [CrossRef] [PubMed]
28. Kuang, Y.; Chen, C.; Kirsch, D.; Hu, L. Thick Electrode Batteries: Principles, Opportunities, and Challenges. *Adv. Energy Mater.* **2019**, *9*, 1901457. [CrossRef]
29. Ju, Z.; Zhang, X.; Wu, J.; King, S.T.; Chang, C.-C.; Yan, S.; Xue, Y.; Takeuchi, K.J.; Marschilok, A.C.; Wang, L.; et al. Tortuosity Engineering for Improved Charge Storage Kinetics in High-Areal-Capacity Battery Electrodes. *Nano Lett.* **2022**, *22*, 6700–6708. [CrossRef]
30. Sun, K.; Wei, T.-S.; Ahn, B.Y.; Seo, J.Y.; Dillon, S.J.; Lewis, J.A. 3D Printing of Interdigitated Li-Ion Microbattery Architectures. *Adv. Mater.* **2013**, *25*, 4539–4543. [CrossRef] [PubMed]
31. Zhang, C.; Shen, L.; Shen, J.; Liu, F.; Chen, G.; Tao, R.; Ma, S.; Peng, Y.; Lu, Y. Anion-Sorbent Composite Separators for High-Rate Lithium-Ion Batteries. *Adv. Mater.* **2019**, *31*, e1808338. [CrossRef]
32. Sander, J.S.; Erb, R.M.; Li, L.; Gurijala, A.; Chiang, Y.-M. High-performance battery electrodes via magnetic templating. *Nat. Energy* **2016**, *1*, 16099. [CrossRef]
33. Billaud, J.; Bouville, F.; Magrini, T.; Villevieille, C.; Studart, A.R. Correction: Corrigendum: Magnetically aligned graphite electrodes for high-rate performance Li-ion batteries. *Nat. Energy* **2017**, *2*, 17061. [CrossRef]
34. Xu, J.; Wang, X.; Yuan, N.; Hu, B.; Ding, J.; Ge, S. Graphite-based lithium ion battery with ultrafast charging and discharging and excellent low temperature performance. *J. Power Sources* **2019**, *430*, 74–79. [CrossRef]
35. Zhang, M.; Song, X.; Ou, X.; Tang, Y. Rechargeable batteries based on anion intercalation graphite cathodes. *Energy Storage Mater.* **2019**, *16*, 65–84. [CrossRef]
36. Cai, W.; Yao, Y.-X.; Zhu, G.-L.; Yan, C.; Jiang, L.-L.; He, C.; Huang, J.-Q.; Zhang, Q. A review on energy chemistry of fast-charging anodes. *Chem. Soc. Rev.* **2020**, *49*, 3806–3833. [CrossRef] [PubMed]
37. Feng, Y.; Zhou, L.; Ma, H.; Wu, Z.; Zhao, Q.; Li, H.; Zhang, K.; Chen, J. Challenges and advances in wide-temperature rechargeable lithium batteries. *Energy Environ. Sci.* **2022**, *15*, 1711–1759. [CrossRef]
38. Liu, Y.; Yang, B.; Dong, X.; Wang, Y.; Xia, Y. A Simple Prelithiation Strategy to Build a High-Rate and Long-Life Lithium-Ion Battery with Improved Low-Temperature Performance. *Angew. Chem. Int. Ed.* **2017**, *56*, 16606–16610. [CrossRef]
39. Kim, N.; Chae, S.; Ma, J.; Ko, M.; Cho, J. Fast-charging high-energy lithium-ion batteries via implantation of amorphous silicon nanolayer in edge-plane activated graphite anodes. *Nat. Commun.* **2017**, *8*, 812. [CrossRef] [PubMed]
40. Yan, Y.; Ben, L.; Zhan, Y.; Huang, X. Nano-Sn embedded in expanded graphite as anode for lithium ion batteries with improved low temperature electrochemical performance. *Electrochim. Acta* **2016**, *187*, 186–192. [CrossRef]
41. Zhang, X.; Zhang, Z.; Hu, F.; Li, D.; Zhou, D.; Jing, P.; Du, F.; Qu, S. Carbon-Dots-Derived 3D Highly Nitrogen-Doped Porous Carbon Framework for High-Performance Lithium Ion Storage. *ACS Sustain. Chem. Eng.* **2019**, *7*, 9848–9856. [CrossRef]
42. Mancini, M.; Nobili, F.; Dsoke, S.; D’amico, F.; Tossici, R.; Croce, F.; Marassi, R. Lithium intercalation and interfacial kinetics of composite anodes formed by oxidized graphite and copper. *J. Power Sources* **2009**, *190*, 141–148. [CrossRef]
43. Markevich, E.; Salitra, G.; Aurbach, D. Low Temperature Performance of Amorphous Monolithic Silicon Anodes: Comparative Study of Silicon and Graphite Electrodes. *J. Electrochem. Soc.* **2016**, *163*, A2407–A2412. [CrossRef]
44. Tan, L.; Hu, R.; Zhang, H.; Lan, X.; Liu, J.; Wang, H.; Yuan, B.; Zhu, M. Subzero temperature promotes stable lithium storage in  $S_nO_2$ . *Energy Storage Mater.* **2021**, *36*, 242–250. [CrossRef]
45. Meng, Q.; Chen, F.; Hao, Q.; Li, N.; Sun, X. Nb-doped  $Li_4Ti_5O_{12}$ - $TiO_2$  hierarchical microspheres as anode materials for high-performance Li-ion batteries at low temperature. *J. Alloy. Compd.* **2021**, *885*, 160842. [CrossRef]
46. Hu, B.; Zhou, X.; Xu, J.; Wang, X.; Yuan, N.; Ge, S.; Ding, J. Excellent Rate and Low Temperature Performance of Lithium-Ion Batteries based on Binder-Free  $Li_4Ti_5O_{12}$  Electrode. *Chemelectrochem* **2020**, *7*, 716–722. [CrossRef]
47. Zhang, H.; Yang, Y.; Xu, H.; Wang, L.; Lu, X.; He, X.  $Li_4Ti_5O_{12}$  spinel anode: Fundamentals and advances in rechargeable batteries. *Infomat* **2022**, *4*, e12228. [CrossRef]
48. Umirov, N.; Yamada, Y.; Munakata, H.; Kim, S.-S.; Kanamura, K. Analysis of intrinsic properties of  $Li_4Ti_5O_{12}$  using single-particle technique. *J. Electroanal. Chem.* **2019**, *855*, 113514. [CrossRef]
49. Pohjalainen, E.; Rauhala, T.; Valkeapää, M.; Kallioinen, J.; Kallio, T. Effect of  $Li_4Ti_5O_{12}$  Particle Size on the Performance of Lithium Ion Battery Electrodes at High C-Rates and Low Temperatures. *J. Phys. Chem. C* **2015**, *119*, 2277–2283. [CrossRef]
50. Subburaj, T.; Brevet, W.; Farmakis, F.; Tsiplikides, D.; Balomenou, S.; Stratakis, N.; Elmasides, C.; Samaniego, B.; Nestoridi, M. Silicon/ $LiNi_{0.8}Co_{0.15}Al_{0.05}O_2$  lithium-ion pouch cells charging and discharging at 40 °C temperature. *Electrochim. Acta* **2020**, *354*, 136652. [CrossRef]

51. Luo, H.; Wang, Y.; Feng, Y.-H.; Fan, X.-Y.; Han, X.; Wang, P.-F. Lithium-Ion Batteries under Low-Temperature Environment: Challenges and Prospects. *Materials* **2022**, *15*, 8166. [[CrossRef](#)]
52. Parfeneva, A.V.; Rumyantsev, A.M.; Lozhkina, D.A.; Maximov, M.Y.; Astrova, E.V. Influence of Fluoroethylene Carbonate in the Composition of an Aprotic Electrolyte on the Electrochemical Characteristics of LIB&rsquos Anodes Based on Carbonized Nanosilicon. *Batteries* **2022**, *8*, 91.
53. Miyazaki, R.; Hihara, T. Charge-discharge performances of Sn powder as a high capacity anode for all-solid-state lithium batteries. *J. Power Sources* **2019**, *427*, 15–20. [[CrossRef](#)]
54. Liang, S.; Cheng, Y.-J.; Zhu, J.; Xia, Y.; Müller-Buschbaum, P. A Chronicle Review of Nonsilicon (Sn, Sb, Ge)-Based Lithium/Sodium-Ion Battery Alloying Anodes. *Small Methods* **2020**, *4*, 2000218. [[CrossRef](#)]
55. Liu, K.; Meng, X.; Yan, L.; Fan, M.; Wu, Y.; Li, C.; Ma, T. Sn/SnO<sub>x</sub> core-shell structure encapsulated in nitrogen-doped porous carbon frameworks for enhanced lithium storage. *J. Alloys Compd.* **2022**, *896*, 163009. [[CrossRef](#)]
56. Ramasubramanian, B.; Sundarrajan, S.; Chellappan, V.; Reddy, M.V.; Ramakrishna, S.; Zaghib, K. Recent Development in Carbon-LiFePO<sub>4</sub> Cathodes for Lithium-Ion Batteries: A Mini Review. *Batteries* **2022**, *8*, 133. [[CrossRef](#)]
57. Cao, R.; Fan, W.; Li, C. In Situ Carbon-Coated NCM622 through CFx for Lithium-Ion Batteries with High Cycling Stability. *J. Electrochem. Soc.* **2019**, *166*, A3348–A3353. [[CrossRef](#)]
58. Jin, Y.; Yu, H.; Liang, X.H. Understanding the roles of atomic layer deposition in improving the electrochemical performance of lithium-ion batteries. *Appl. Phys. Rev.* **2021**, *8*, 031301. [[CrossRef](#)]
59. Asif, M.; Rashad, M.; Ali, Z.; Qiu, H.L.; Li, W.; Pan, L.J.; Hou, Y.L. Ni-doped MnO<sub>2</sub>/CNT nanoarchitectures as a cathode material for ultra-long life magnesium/lithium hybrid ion batteries. *Mater. Today Energy* **2018**, *10*, 108–117. [[CrossRef](#)]
60. Zhao, B.; Xie, J.; Zhuang, H.; Liu, X.; Li, W.; Hu, X.; Jiang, Y.; Zhang, J. Improved low-temperature performance of surface modified lithium-rich Li<sub>1.2</sub>Ni<sub>0.13</sub>Co<sub>0.13</sub>Mn<sub>0.54</sub>O<sub>2</sub> cathode materials for lithium ion batteries. *Solid State Ion.* **2020**, *347*, 115245. [[CrossRef](#)]
61. Sun, Z.; Jiao, L.; Fan, Y.; Li, F.; Wang, D.; Han, D.; Niu, L. Industrialization of tailoring spherical cathode material towards high-capacity, cycling-stable and superior low temperature performance for lithium-ion batteries. *RSC Adv.* **2016**, *6*, 97818–97824. [[CrossRef](#)]
62. Bi, K.; Zhao, S.-X.; Huang, C.; Nan, C.-W. Improving low-temperature performance of spinel LiNi<sub>0.5</sub>Mn<sub>1.5</sub>O<sub>4</sub> electrode and LiNi<sub>0.5</sub>Mn<sub>1.5</sub>O<sub>4</sub>/Li<sub>4</sub>Ti<sub>5</sub>O<sub>12</sub> full-cell by coating solid-state electrolyte Li-Al-Ti-P-O. *J. Power Sources* **2018**, *389*, 240–248. [[CrossRef](#)]
63. Zhang, W.; Sun, X.; Tang, Y.; Xia, H.; Zeng, Y.; Qiao, L.; Zhu, Z.; Lv, Z.; Zhang, Y.; Ge, X.; et al. Lowering Charge Transfer Barrier of LiMn<sub>2</sub>O<sub>4</sub> via Nickel Surface Doping to Enhance Li<sup>+</sup> Intercalation Kinetics at Subzero Temperatures. *J. Am. Chem. Soc.* **2019**, *141*, 14038–14042. [[CrossRef](#)]
64. Zhang, H.; Xu, Y.; Zhao, C.; Yang, X.; Jiang, Q. Effects of carbon coating and metal ions doping on low temperature electrochemical properties of LiFePO<sub>4</sub> cathode material. *Electrochim. Acta* **2012**, *83*, 341–347. [[CrossRef](#)]
65. Nagasubramanian, G. Electrical characteristics of 18650 Li-ion cells at low temperatures. *J. Appl. Electrochem.* **2001**, *31*, 99–104. [[CrossRef](#)]
66. Kim, J.W.; Jung, K.; Yim, T. Dually-functionalized Ni-rich layered oxides for high-capacity lithium-ion batteries. *J. Mater. Sci. Technol.* **2021**, *86*, 70–76. [[CrossRef](#)]
67. Tan, S.; Wang, L.; Bian, L.; Xu, J.; Ren, W.; Hu, P.; Chang, A. Highly enhanced low temperature discharge capacity of LiNi<sub>1/3</sub>Co<sub>1/3</sub>Mn<sub>1/3</sub>O<sub>2</sub> with lithium boron oxide glass modification. *J. Power Sources* **2015**, *277*, 139–146. [[CrossRef](#)]
68. Li, G.; Huang, Z.; Zuo, Z.; Zhang, Z.; Zhou, H. Understanding the trace Ti surface doping on promoting the low temperature performance of LiNi<sub>1/3</sub>Co<sub>1/3</sub>Mn<sub>1/3</sub>O<sub>2</sub> cathode. *J. Power Sources* **2015**, *281*, 69–76. [[CrossRef](#)]
69. Bakierska, M.; Chudzik, K.; Świętosławski, M.; Klejna, S.; Kubicka, M.; Marciszko-Wiąckowska, M.; Gajewska, M.; Walas, S.; Molenda, M. Reversible Cation-Mediated Anionic Redox in Defect Spinel Structure for High Power Batteries. *Adv. Funct. Mater.* **2022**, *32*, 2108278. [[CrossRef](#)]
70. Oh, H.H.; Joo, J. Colloidal synthesis of monodisperse ultrathin LiFePO<sub>4</sub> nanosheets for Li-ion battery cathodes. *Korean J. Chem. Eng.* **2021**, *38*, 1052–1058. [[CrossRef](#)]
71. Kim, C.; Yang, Y.; Ha, D.; Kim, D.H.; Kim, H. Crystal alignment of a LiFePO<sub>4</sub> cathode material for lithium ion batteries using its magnetic properties. *RSC Adv.* **2019**, *9*, 31936–31942. [[CrossRef](#)]
72. Zhu, Z.; Tang, Y.; Lv, Z.; Wei, J.; Zhang, Y.; Wang, R.; Zhang, W.; Xia, H.; Ge, M.; Chen, X. Fluoroethylene Carbonate Enabling a Robust LiF-rich Solid Electrolyte Interphase to Enhance the Stability of the MoS<sub>2</sub> Anode for Lithium-Ion Storage. *Angew. Chem. Int. Ed.* **2018**, *57*, 3656–3660. [[CrossRef](#)]
73. Wang, S.; Chen, X.; Zhang, Y.; Zheng, S. Lithium adsorption from brine by iron-doped titanium lithium ion sieves. *Particuology* **2018**, *41*, 40–47. [[CrossRef](#)]
74. Alhammadi, A.S.; Yun, H.J.; Choi, D. Investigation of LiFePO<sub>4</sub>/MWCNT cathode-based half-cell lithium-ion batteries in subzero temperature environments. *Ionics* **2023**, *29*, 2163–2174. [[CrossRef](#)]
75. Li, Y.; Wang, L.; Liang, F.; Yao, Y.; Zhang, K. Enhancing high rate performance and cyclability of LiFePO<sub>4</sub> cathode materials for lithium ion batteries by boron doping. *J. Alloys Compd.* **2021**, *880*, 160560. [[CrossRef](#)]
76. Cui, X.; Tuo, K.; Xie, Y.; Li, C.; Zhao, D.; Yang, L.; Fu, X.; Li, S. Investigation on electrochemical performance at the low temperature of LFP/C-P composite based on phosphorus doping carbon network. *Ionics* **2020**, *26*, 3795–3808. [[CrossRef](#)]

77. Zhao, N.; Li, Y.; Zhao, X.; Zhi, X.; Liang, G. Effect of particle size and purity on the low temperature electrochemical performance of LiFePO<sub>4</sub>/C cathode material. *J. Alloys Compd.* **2016**, *683*, 123–132. [[CrossRef](#)]
78. Wang, J.; Zhang, Y.; Yi, M.; Shen, Z.; Liu, L.; Liu, H.; Zhang, X. Coating LiFePO<sub>4</sub> with Conductive Nanodots by Magnetron Sputtering: Toward High-Performance Cathode for Lithium-Ion Batteries. *Energy Technol.* **2019**, *7*, 1800634. [[CrossRef](#)]
79. Peng, Y.; Tan, R.; Ma, J.; Li, Q.; Wang, T.; Duan, X. Electrospun Li<sub>3</sub>V<sub>2</sub>(PO<sub>4</sub>)<sub>3</sub> nanocubes/carbon nanofibers as free-standing cathodes for high-performance lithium-ion batteries. *J. Mater. Chem. A* **2019**, *7*, 14681–14688. [[CrossRef](#)]
80. Luo, Y.; Xu, X.; Zhang, Y.; Pi, Y.; Zhao, Y.; Tian, X.; An, Q.; Wei, Q.; Mai, L. Hierarchical Carbon Decorated Li<sub>3</sub>V<sub>2</sub>(PO<sub>4</sub>)<sub>3</sub> as a Bicontinuous Cathode with High-Rate Capability and Broad Temperature Adaptability. *Adv. Energy Mater.* **2014**, *4*, 1400107. [[CrossRef](#)]
81. Dong, X.; Yang, Y.; Wang, B.; Cao, Y.; Wang, N.; Li, P.; Wang, Y.; Xia, Y. Low-Temperature Charge/Discharge of Rechargeable Battery Realized by Intercalation Pseudocapacitive Behavior. *Adv. Sci.* **2020**, *7*, 2000196. [[CrossRef](#)]
82. Zhang, X.; Sun, X.; Li, X.; Hu, X.; Cai, S.; Zheng, C. Recent progress in rate and cycling performance modifications of vanadium oxides cathode for lithium-ion batteries. *J. Energy Chem.* **2021**, *59*, 343–363. [[CrossRef](#)]
83. Sides, C.R.; Martin, C.R. Nanostructured Electrodes and the Low-Temperature Performance of Li-Ion Batteries. *Adv. Mater.* **2005**, *17*, 125–128. [[CrossRef](#)]
84. Von Wald Cresce, A.; Xu, K. Aqueous lithium-ion batteries. *Carbon Energy* **2021**, *3*, 721–751. [[CrossRef](#)]
85. Chen, L.; Cao, L.; Ji, X.; Hou, S.; Li, Q.; Chen, J.; Yang, C.; Eidson, N.; Wang, C. Enabling safe aqueous lithium ion open batteries by suppressing oxygen reduction reaction. *Nat. Commun.* **2020**, *11*, 2638. [[CrossRef](#)]
86. Ramanujapuram, A.; Yushin, G. Understanding the Exceptional Performance of Lithium-Ion Battery Cathodes in Aqueous Electrolytes at Subzero Temperatures. *Adv. Energy Mater.* **2018**, *8*, 1802624. [[CrossRef](#)]
87. Tron, A.; Jeong, S.; Park, Y.D.; Mun, J. Aqueous Lithium-Ion Battery of Nano-LiFePO<sub>4</sub> with Antifreezing Agent of Ethyleneglycol for Low-Temperature Operation. *ACS Sustain. Chem. Eng.* **2019**, *7*, 14531–14538. [[CrossRef](#)]
88. Kühnel, R.-S.; Böckenfeld, N.; Passerini, S.; Winter, M.; Balducci, A. Mixtures of ionic liquid and organic carbonate as electrolyte with improved safety and performance for rechargeable lithium batteries. *Electrochim. Acta* **2011**, *56*, 4092–4099. [[CrossRef](#)]
89. Ue, M.; Takeda, M.; Toriumi, A.; Kominato, A.; Hagiwara, R.; Ito, Y. Application of Low-Viscosity Ionic Liquid to the Electrolyte of Double-Layer Capacitors. *J. Electrochem. Soc.* **2003**, *150*, A499–A502. [[CrossRef](#)]
90. Liu, B.; Li, Q.; Engelhard, M.H.; He, Y.; Zhang, X.; Mei, D.; Wang, C.; Zhang, J.-G.; Xu, W. Constructing Robust Electrode/Electrolyte Interphases to Enable Wide Temperature Applications of Lithium-Ion Batteries. *ACS Appl. Mater. Interfaces* **2019**, *11*, 21496–21505. [[CrossRef](#)]
91. Zhang, S.S.; Xu, K.; Jow, T.R. A new approach toward improved low temperature performance of Li-ion battery. *Electrochem. Commun.* **2002**, *4*, 928–932. [[CrossRef](#)]
92. Deiner, L.J.; Bezerra, C.A.G.; Howell, T.G.; Powell, A.S. Digital Printing of Solid-State Lithium-Ion Batteries. *Adv. Eng. Mater.* **2019**, *21*, 1900737. [[CrossRef](#)]
93. Ke, X.; Wang, Y.; Ren, G.; Yuan, C. Towards rational mechanical design of inorganic solid electrolytes for all-solid-state lithium ion batteries. *Energy Storage Mater.* **2020**, *26*, 313–324. [[CrossRef](#)]
94. Lin, Z.; Liu, J. Low-temperature all-solid-state lithium-ion batteries based on a di-cross-linked starch solid electrolyte. *RSC Adv.* **2019**, *9*, 34601–34606. [[CrossRef](#)]
95. Li, X.; Hou, Q.; Huang, W.; Xu, H.-S.; Wang, X.; Yu, W.; Li, R.; Zhang, K.; Wang, L.; Chen, Z.; et al. Solution-Processable Covalent Organic Framework Electrolytes for All-Solid-State Li–Organic Batteries. *ACS Energy Lett.* **2020**, *5*, 3498–3506. [[CrossRef](#)]
96. Tang, X.; Lv, S.; Jiang, K.; Zhou, G.; Liu, X. Recent development of ionic liquid-based electrolytes in lithium-ion batteries. *J. Power Source* **2022**, *542*, 231792. [[CrossRef](#)]
97. Hu, Y.; Yu, L.; Meng, T.; Zhou, S.; Sui, X.; Hu, X. Hybrid Ionogel Electrolytes for Advanced Lithium Secondary Batteries: Developments and Challenges. *Chem.—Asian J.* **2022**, *17*, e202200794. [[CrossRef](#)] [[PubMed](#)]
98. Francis, C.F.J.; Kyriazis, I.L.; Best, A.S. Lithium-Ion Battery Separators for Ionic-Liquid Electrolytes: A Review. *Adv. Mater.* **2020**, *32*, e1904205. [[CrossRef](#)] [[PubMed](#)]
99. Aguilera, L.; Scheers, J.; Matic, A. Enhanced low-temperature ionic conductivity via different Li<sup>+</sup> solvated clusters in organic solvent/ionic liquid mixed electrolytes. *Phys. Chem. Chem. Phys.* **2016**, *18*, 25458–25464. [[CrossRef](#)]
100. Chen, M.; Wu, J.; Ye, T.; Ye, J.; Zhao, C.; Bi, S.; Yan, J.; Mao, B.; Feng, G. Adding salt to expand voltage window of humid ionic liquids. *Nat. Commun.* **2020**, *11*, 5809. [[CrossRef](#)]
101. Zhang, J.; Yao, X.; Misra, R.K.; Cai, Q.; Zhao, Y. Progress in electrolytes for beyond-lithium-ion batteries. *J. Mater. Sci. Technol.* **2020**, *44*, 237–257. [[CrossRef](#)]
102. Gao, Z.; Rao, S.; Zhang, T.; Li, W.; Yang, X.; Chen, Y.; Zheng, Y.; Ding, Y.; Dong, T.; Li, S. Design Strategies of Flame-Retardant Additives for Lithium Ion Electrolyte. *J. Electrochem. Energy Convers. Storage* **2022**, *19*, 030910. [[CrossRef](#)]
103. Liu, Y.-K.; Zhao, C.-Z.; Du, J.; Zhang, X.-Q.; Chen, A.-B.; Zhang, Q. Research Progresses of Liquid Electrolytes in Lithium-Ion Batteries. *Small* **2023**, *19*, 2205315. [[CrossRef](#)]
104. Dong, X.; Lin, Y.; Li, P.; Ma, Y.; Huang, J.; Bin, D.; Wang, Y.; Qi, Y.; Xia, Y. High-Energy Rechargeable Metallic Lithium Battery at  $-70^{\circ}\text{C}$  Enabled by a Cosolvent Electrolyte. *Angew. Chem. Int. Engl. Ed.* **2019**, *58*, 5623–5627. [[CrossRef](#)]
105. Luo, D.; Li, M.; Zheng, Y.; Ma, Q.; Gao, R.; Zhang, Z.; Dou, H.; Wen, G.; Shui, L.; Yu, A.; et al. Electrolyte Design for Lithium Metal Anode-Based Batteries Toward Extreme Temperature Application. *Adv. Sci.* **2021**, *8*, e2101051. [[CrossRef](#)]

106. Su, X.; Xu, Y.; Wu, Y.; Li, H.; Yang, J.; Liao, Y.; Qu, R.; Zhang, Z. Liquid electrolytes for low-temperature lithium batteries: Main limitations, current advances, and future perspectives. *Energy Storage Mater.* **2023**, *56*, 642–663. [[CrossRef](#)]
107. Phiri, I.; Ko, S.; Kim, S.; Afrifah, V.A.; Lee, K.; Kim, S.H.; Ko, J.M. Zwitterionic osmolyte-inspired additives as scavengers and low temperature performance enhancers for lithium ion batteries. *Mater. Lett.* **2021**, *288*, 129366. [[CrossRef](#)]
108. Xu, G.; Huang, S.; Cui, Z.; Du, X.; Wang, X.; Lu, D.; Shangguan, X.; Ma, J.; Han, P.; Zhou, X.; et al. Functional additives assisted ester-carbonate electrolyte enables wide temperature operation of a high-voltage (5 V-Class) Li-ion battery. *J. Power Source* **2019**, *416*, 29–36. [[CrossRef](#)]
109. He, H.; Wang, Y.; Li, M.; Qiu, J.; Wen, Y.; Chen, J. Effect of fluoroethylene carbonate additive on the low-temperature performance of lithium-ion batteries. *J. Electroanal. Chem.* **2022**, *925*, 116870. [[CrossRef](#)]
110. Klein, S.; Harte, P.; van Wickeren, S.; Borzutzki, K.; Röser, S.; Bärmann, P.; Nowak, S.; Winter, M.; Placke, T.; Kasnatscheew, J. Re-evaluating common electrolyte additives for high-voltage lithium ion batteries. *Cell Rep. Phys. Sci.* **2021**, *2*, 100521. [[CrossRef](#)]
111. Kalantzopoulos, G.N.; Lundvall, F.; Checchia, S.; Lind, A.; Wragg, D.S.; Fjellvåg, H.; Arstad, B. In Situ Flow MAS NMR Spectroscopy and Synchrotron PDF Analyses of the Local Response of the Brønsted Acidic Site in SAPO-34 during Hydration at Elevated Temperatures. *ChemPhysChem* **2017**, *19*, 519–528. [[CrossRef](#)]
112. Hu, X.; Zheng, Y.; Howey, D.A.; Perez, H.; Foley, A.; Pecht, M. Battery warm-up methodologies at subzero temperatures for automotive applications: Recent advances and perspectives. *Prog. Energy Combust. Sci.* **2020**, *77*, 100806. [[CrossRef](#)]
113. He, F.; Li, X.; Zhang, G.; Zhong, G.; He, J. Experimental investigation of thermal management system for lithium ion batteries module with coupling effect by heat sheets and phase change materials. *Int. J. Energy Res.* **2018**, *42*, 3279–3288. [[CrossRef](#)]
114. Ruan, H.; Sun, B.; Cruden, A.; Zhu, T.; Jiang, J.; He, X.; Su, X.; Ghoniem, E. Optimal external heating resistance enabling rapid compound self-heating for lithium-ion batteries at low temperatures. *Appl. Therm. Eng.* **2021**, *200*, 117536. [[CrossRef](#)]
115. Wu, S.; Xiong, R.; Li, H.; Nian, V.; Ma, S. The state of the art on preheating lithium-ion batteries in cold weather. *J. Energy Storage* **2020**, *27*, 101059. [[CrossRef](#)]

**Disclaimer/Publisher's Note:** The statements, opinions and data contained in all publications are solely those of the individual author(s) and contributor(s) and not of MDPI and/or the editor(s). MDPI and/or the editor(s) disclaim responsibility for any injury to people or property resulting from any ideas, methods, instructions or products referred to in the content.